Strål säkerhets myndigheten
Swedish Radiation Safety Authority

Authors: Gustav Holmer
Will Daniels
Tommy Zettervall

Research

2017:29

Evaluation of the simulation software CIVA for qualification purpose

Report number: 2017:29 **ISSN:** 2000-0456
Available at www.stralsakerhetsmyndigheten.se

SSM perspective

Background

Modeling is an important tool within NDT, partly to develop and optimize testing technologies, but also within the Qualification Body's activities to assess technical verifications and perform parameter studies. SSM has supported university research in the area for many years and, among other things, in the development of a software for ultrasound modeling. In addition, the accredited NDE laboratories are increasingly using software for modeling inspection situations.

CIVA, developed by French CEA, is the commercially most successful software in simulation of NDT situations. The program according to the supplier can handle different materials, geometries, cladding and anisotropy in arbitrary symmetry and orientation. Even simulation of material structures, different probe types and defects with arbitrary shape, size and orientation can be simulate. UT, ET and RT are the NDT methods that the program can simulate. A project was started to evaluate the usability of the software within qualification projects.

The work performed within this research report only handles with the UT-module of the simulation software. The intended purpose with CIVA is to provide a tool for developing and optimizing probe design, enhancing qualification and supply help in analysis of inspection results.

The work has been carried out as collaboration between SQC (Swedish Qualification Body) and AMEC.

Objective

The purpose of this project has been to evaluate the usability of the simulation software CIVA within qualification projects.

CIVA software is used more and more in connection with qualification of NDT inspection systems, both during technique development and as a part of the technical justifications. The Qualification Body has to know the boundaries of such simulation tool to be able to assess the simulation results presented in a technical justification. Other areas where the Qualification Body can use this simulation tool (if verified) are parameter studies. Parameter studies can be used for review of important parameters, in order to find out limit values as well as which parameters are most important for the inspection system. In addition, optimization of defect content for the manufacture of test blocks can be done.

Results

The results of the work performed in this project indicate that simulations and experiments matches rather well.

The largest discrepancy between the simulations and experiments is noise or rather signal to noise ratio. Noise caused by the material structure can be modelled in CIVA but as a separate layer, which is super positioned on top of the defect response simulation, meaning

that the defect response is not affected by the noise. If a noise simulation is used, it must be used together with additional attenuation modeling or else the result will be a non-conservative signal to noise ratio for any given indication. No simulations of noise or attenuation were made within this project.

It is not possible to simulate a complete inspection, or validate an inspection procedure by simulations with CIVA at the current time. Both the producer of simulated data and the evaluator must have great knowledge about the CIVA software to be able to draw the right conclusions from the results. Whether CIVA can be used in qualifications or not is a question of the purpose of the simulation and also the extent of the usage of simulated data.

Need for further research

Noise is a significant part of a qualified procedure and the corresponding technical justification. Defects responses are often evaluated in relation to the surrounding noise levels rather than an arbitrary reference target, such as a notch or SDH. Future work needs to be done focusing in CIVA capability to simulate noise and attenuation.

Project information

Contact person SSM: Giselle García Roldán
Reference: SSM2010-299, 2037031-03

Strål
säkerhets
myndigheten
Swedish Radiation Safety Authority

Authors: Gustav Holmer[1], Will Daniels[2], Tommy Zettervall[1]
[1] SQC Swedish Qualification Centre, Täby Sweden
[2] AMEC Foster Wheeler, Birchwood, United Kingdom

2017:29

Evaluation of the simulation software CIVA for qualification purpose

Date: November 2017
Report number: 2017:29 **ISSN:** 2000-0456
Available at www.stralsakerhetsmyndigheten.se

This report concerns a study which has been conducted for the Swedish Radiation Safety Authority, SSM. The conclusions and viewpoints presented in the report are those of the author/authors and do not necessarily coincide with those of the SSM.

Table of contents

List of abbreviations

Abbreviation	Explanation
AMEC	Amec Foster Wheeler plc
BAM	Bundesanstalt für Materialforschung und –prüfung
B-Scan	Graphic presentation of UT-data as a side view
CAD	Computer Aided Design
CEA	Commissariat à l'énergie atomique
D/A	Digital / Analog
EDM	Electric Discharge Machining
ET	Eddy Current Testing
FBH	Flat Bottomed Hole
GTD	Geometrical Theory of Diffraction
HIP	Hot Isostatic Pressure
ISI	In Service Inspection
MOD	Ministry of Defence
NDE	Non Destructive Evaluation
NDT	Non Destructive Testing
NPP	Nuclear Power Plant
PA	Phased Array
PCS	Probe Centre Separation
PE	Pulse Echo
POD	Probability of Detection
RT	Radiographic Testing
SCC	Stress Corrosion Crack
SDH	Side Drilled Hole
SG	Steam Generator
SKI	Statens KärnkraftsInspektion
SOV	Separation of Variables
SQC	Swedish Qualification Centre AB
SSM	Swedish Radiation Safety Authority
TOFD	Time Of Flight Diffraction
TRL	Transmit Receive Longitudinal
UK	United Kingdom
UT	Ultrasonic Testing
VTT	Technical Research Centre of Finland

1. Introduction

Purpose

The purpose of this report and the work leading to it has been to evaluate the usability of the simulation software CIVA within qualification projects. Simulation software are used more and more as a tool during technique development and a part of technical justifications. In order to be able to assess the statements given as a result of simulations in a technical justification one has to know the boundaries of the simulation tools´ reliable performance. The work resulting in this report has been carried out with CIVA as it is the commercially most successful software and thereby the one most likely to appear in qualification documentation.

Nondestructive testing and evaluation in nuclear power plants differ from inspections in the conventional industry in regard to the defects that are sought, and also the actions following when a defect is found. When a defect is found in conventional industry the object that is flawed is repaired and re-inspected. Once a weld is considered free from defects it is generally not inspected again due to the fact that after manufacturing the risk of cracks decrease significantly. As repairs are very costly in nuclear power plants and the cost of a component failure even higher objects critical to plant safety are subject to periodic inspections. These inspections are designed to detect, size and characterize defects of different types with different characteristics in order to be able to assess the remaining life of the component before the defect becomes critical and a repair has to be made. These cracks with known damage mechanisms are typically harder to detect and characterize than typical manufacturing defects sought in conventional industry.

The intention of the verification process is to devise and apply a series of tests which can be used to:

- estimate the likely accuracy of the model prediction;
- reach a view on the regions of applicability of the model

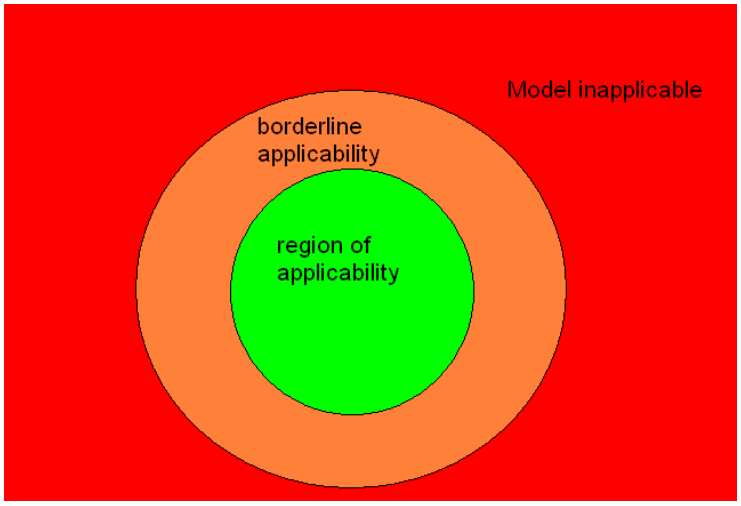

Figure 1 Region of applicability concept

In general terms it can be expected that any model will have a region of problem space where its founding theory and assumptions are valid, a region where assumptions are starting to be breached and a region where it should not be applied. This concept is shown in Figure 1.

Implementation

The work has been carried out as collaboration between SQC and AMEC, sponsored by SSM and MOD respectively. The general idea has been to identify a number of specific cases relevant to qualification work and set up a series of experiments on specimens with various shapes and reflectors with corresponding simulation runs. The results are then compared in terms of amplitude, echo dynamic and signal appearance. Various types of signals that are common in ultrasonic inspections have been investigated, such as corner trap responses, tip diffraction (both TOFD and PE), Rayleigh waves and SDH and FBH specular reflection. Several different probes have been used.

The model verification activities are divided into five different partial phases. Each phase is divided into a number of different tasks with specific purposes. The experiments are described in detail in the Experiments and simulations chapter. After completion of each phase a phase report has been produced that summarizes the obtained results, but no conclusions were presented in these reports. It was decided to draw the conclusions after the whole body of work was completed, to inaugurate the whole picture. However, when larger issues have occurred, some significant work has been carried out in order to find the root cause of the issue.

	Model capability to be assessed
Phase 1	Response prediction for simple/smooth defects in simple materials and probe modeling
Phase 2	Geometry handling with model
Phase 3	Complex materials – austenitic welds, inconels, dissimilar metal welds
Phase 4	Rough defects in simple materials
Phase 5	Rough defects in complex materials

Table 1 Comparison phases

The difference between simple/smooth defects and rough defects stated in Table 1 is that simple/smooth defects are typically artificial defects or an ideal fatigue crack. Rough defects are the type of defects that are typically service induced, with a clear morphology, following grain structure or other irregularities. By simple materials means carbon steel or stainless parent material that shows isotropic behavior. Complex materials show anisotropic behavior with significant influence on the sound beam giving effects such as large scattering, beam deflection and increased noise.

There are options within CIVA to model attenuation caused by the material, in addition to the sound beam divergence. This attenuation can easily be measured if your samples´ geometry will allow it and two identical probes can be used. This presents an issue also mentioned in chapter 3, Ultrasonic equipment. When it comes to noise and specifically grain noise caused by coarse grain structure and anisotropic materials it can also be modelled if the grain structure is known and defined in CIVA.

However, this noise caused by the material structure is modelled as a separate layer which is super positioned on top of the defect response simulation, meaning that the defect response is not affected by the noise. If a noise simulation is used, it must be used together with additional attenuation modeling as mentioned above or else the result will be a non-conservative signal to noise ratio for any give indication.

Because of the issues with noise and attenuation, no consideration of these phenomena has been taken within this project.

2. CIVA

CIVA is a software for simulation of NDT developed by the CEA. The software is capable of simulating UT, ET and RT. The work presented within this report only handles with the UT-module. The intended purpose with CIVA is to provide a tool for developing and optimizing probe design, enhancing qualification and supply help in analysis of inspection results.

When the work leading to this report was started CIVA version 9 was used. Since then version 10 and 11 has been released. This has raised questions concerning whether early simulation results are still valid at the time of publication of the results. To some extent, this has been handled with reruns using CIVA version 11 for selected simulations. No large differences in the result were found, so it was decided that older simulations could be kept without any further action. However, if some errors in older simulations have been found, the new and rectified simulation has always been made with the latest version of the software.

Identification of Regions of Applicability Stated in User Guide

In the user guidance supplied with CIVA version 11 [1], there is some discussion of regions of applicability. The following are extracts from the user guide text:

Section 2.1.1.4, page 217: **UT beam computation in welds and very heterogeneous media:**

"... wavelength of the ultrasonic field has to be small when compared with some characteristic length of the model. Failure to comply can make the calculation unreliable."

A process for overcoming this problem is mentioned if not described.

On page 230 concerning the computation of the incident field, it is stated that the sound field is incompletely modelled in the transducer's acoustic near field.

Page 235: **Main advantages and limitations of the Kirchoff's [sic] approximation:**

"Kirchhoff's approximation is a high frequency approximation, valid when the defect is greater than the wavelength, that is, when ka >>1, where k is the wavenumber and a is the main dimension of the defect."

"The computation of this approximation implicitly assumes that both the transmitter and the receiver belong to the same half-space limited by the defect plane: the incidence and observation angle shall lie in the same side of the flaw, as illustrated on the following figure for a Tandem configuration:

For the first position (top of the figure), both probes are lying on the same side of the flaw, an echo is calculated. For the second position (bottom of the figure), the axis of the receiving probe doesn't lie in the half space defined by the flaw orientation, therefore one cannot predict the echo scattered by the flaw because the Kirchhoff developed model is not applicable (the receiving probe is lying in the so-called 'shadowed area'). "

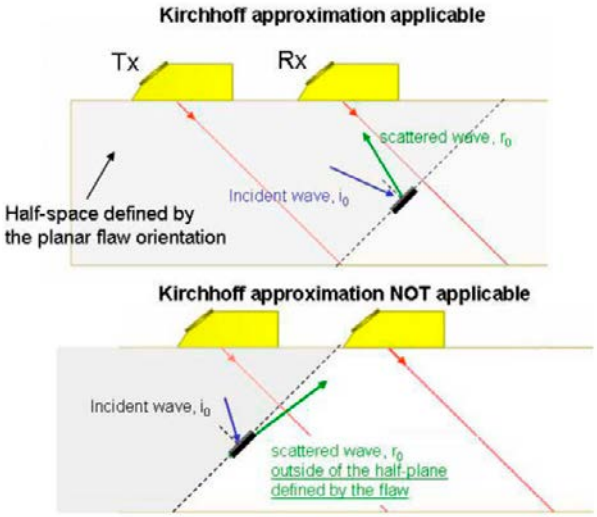

Figure 2 Limitation of Kirchoff model application using two probes in Tandem mode

"Similar limitations occur when using a pair of probes in TOFD inspection (see following figure) for nearly vertical flaws: The Kirchhoff model will soon be not applicable as the orientation of the flaw prevents the axis of the transmitter and receiver probes lying from the same side of the flaw. On the following figure, only the configuration displayed on top can be simulated using the Kirchhoff model."

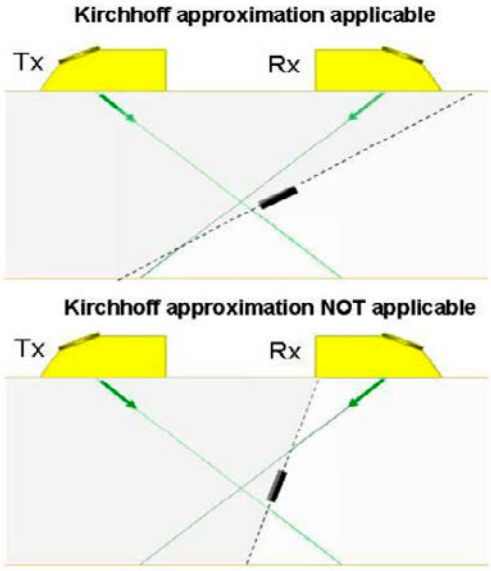

Figure 3 Limitation of Kirchoff application using two probes in TOFD mode

"The Kirchhoff approximation, classically used in NDT modelling, is assumed to give accurate results when the flaw is detected in specular or pseudo-specular mode, i.e. when the observation angle (the angle of the receiver) is close to the "natural" specular reflexion of the incidence wave upon the flaw."

And later on page 237

"The Kirchhoff approximation is, therefore, mostly valid for:
- Specular reflexion over planar or volumetric defects, large compared to the wavelength (large ka, k being the wavenumber and a the characteristic length of the scatterer)"

and on page 238 regarding the corner effect model,

"Tip diffraction echoes from planar defects can be accurately predicted using the Kirchhoff approximation in terms of time of flight, however their amplitudes cannot be quantitatively predicted using the Kirchhoff model. The quantitative error is expected to increase when the scattered direction moves away from the specular direction."

On page 239 regarding GTD

"GTD is also a high frequency approximation, valid when the defect is greater than the wavelength, that is, when ka >>1, where k is the wave number and a is the main dimension of the defect."

On page 265

"Limitations related to the use of superposition and modelled modes are recounted. In summary, the stated limitations are that the Kirchoff and GTD algorithms are suited to calculation of ultrasonic responses for defects which are large compared to the insonifying ultrasound's wavelength and that the calculations are not reliable for defects in the transducer's near field."

Good Practice

The user guide contains a flow diagram, which is presented as good practice for safety critical application assessment as follows:

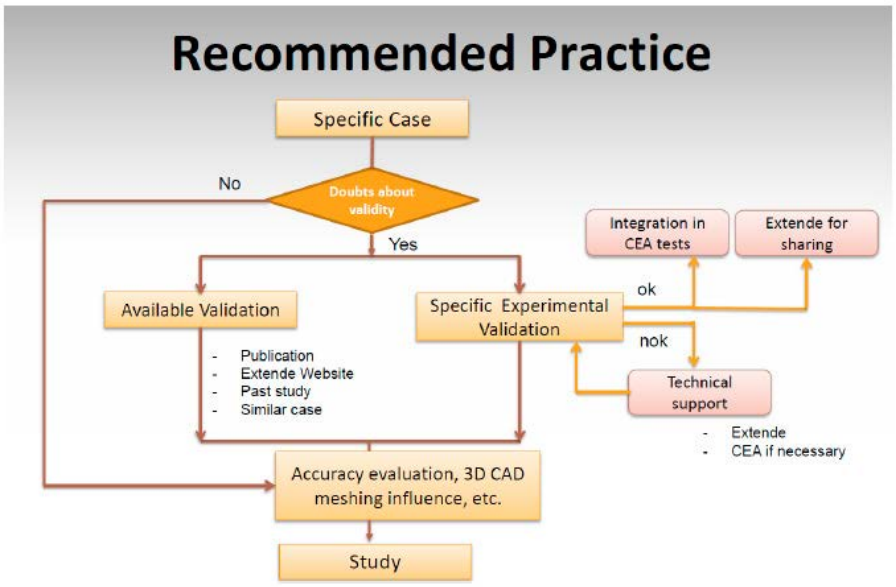

Figure 4 CIVA use best practice

In summary, the stated best practice requires users to examine the validation data sources which are identified as available publications, the provider's website, or the user's own experience for relevant validation information. In the event that no relevant data, it is suggested that the user obtains validation data through "specific experimental validation".

EXTENDE Website

EXTENDE (CIVA's supplier, www.extende.com) maintain a website of validation evidence. The website contains a significant volume of validation work, but does not treat all information relevant to all possible cases of interest within nuclear power plant inspection design and qualification.

3. Ultrasonic equipment

Physical experiments have been carried out both at AMEC and SQC facilities using the following different UT-systems.

	UT Hardware used	UT Software	Task
Phase 1	Peak NDT Micropulse 5	Arraygen	7
	Zetec Z-Scan UT	UltraVision 1.1Q3	1-6
Phase 2	Zetec Z-Scan UT	UltraVision 1.1Q3	1-6
Phase 3	Zetec Z-Scan UT	UltraVision 1.1Q3	
	Zetec Dynaray Lite	UltraVision 3.3R4	
Phase 4	Peak NDT Micropulse 5	N/A	
Phase 5	Peak NDT Micropulse 5	N/A	

Table 2 Ultrasonic equipment

Several different probes were used in the experiments. The probes that were used were chosen with the purpose of the experiment, geometry and material properties in the sample in mind. A limiting factor of probe choice is the amount of available probes available in SQC´s and AMEC´s laboratories. The result is that in all cases an optimal probe for the task may not have been used. The purpose is to compare simulations with experiments, not to obtain the best possible inspection result. Unfortunately the limited selection of probes left the measurement of the samples attenuation impossible.

	Probes used	Type
Phase 1	TRC PCS 30	TOFD
	SWK 45-2	Single crystal angle beam, Shear
	SWK 60-2	Single crystal angle beam, Shear
	SWK 70-2	Single crystal angle beam, Shear
	TRL 45-2	Dual crystal angle beam, Long
	TRL 70-2	Dual crystal angle beam, Long
	64 Element linear array	Phased array
Phase 2	MWK 45-2	Single crystal angle beam, Shear
	MWK 60-2	Single crystal angle beam, Shear
	MWB 45-4	Single crystal angle beam, Shear
	TRL 45-2	Dual crystal angle beam, Long
	QCX 36	Single crystal angle beam, Long
	QCX 45	Single crystal angle beam, Shear
	Wedge 45	Single crystal angle beam, Shear
Phase 3	TRL45-2	Dual crystal angle beam, Long
	TRL60-2	Dual crystal angle beam, Long
	TRL70-2	Dual crystal angle beam, Long
Phase 4	45°S	Single crystal angle beam, Shear
	60°S	Single crystal angle beam, Shear
Phase 5	TRL45-2	Dual crystal angle beam, Long
	TRL60-2	Dual crystal angle beam, Long

Table 3 Ultrasonic probes

4. Error analysis

Data collection was controlled by a procedure authored by SQC and reviewed by AMEC. In what follow amplitude data are reported with respect to a pre-defined side drilled hole reference or geometrical feature of the sample as described in the data collection procedure specific for each experiment.

Anticipated errors

In order to assess the correlation between measured and modelled inspection data, it is necessary to quantify the sensitivity of the response to inspection parameter tolerances. For instance, the defect through wall extent, beam angles, pulse shape, frequency, while controlled, are only known to certain tolerances. The measured data are obtained with equipment parameters and from samples for which the specification is only known to certain tolerances.

An assessment has been performed to establish the likely sensitivity of the modelled result to the likely parameter tolerances. This gives a means for comparing measured and modelled data, and judging the significance of any discrepancies.

The method used was firstly to identify influential parameters, and then evaluate the likely tolerance and concomitant amplitude variation associated with each parameter. The variations were then combined using a partial Monte Carlo error combination approach.

Error due to Digitization

The analogue response signal is digitized in the experimental data used in this study. The digitization is at uniform time steps with discrete amplitude quantization. Two equipment systems have been used in this study. The PE and TOFD system had a 12-bit amplitude resolution and a digitization frequency of 50 MHz.

It means that the amplitude is sampled every $1/(50 \times 10^6)$ seconds and that the equipment's full-scale is sampled in 2^{12} increments. In this experimental programme, phase information is maintained. So one amplitude bit is effectively sacrificed to record the phase (bipolar digitization), so that the amplitude is resolved to $1/2^{11}$ of the equipment's D/A converter full scale. In practice, this means a possibility of underestimating the signal response by up to one amplitude quantization step or one part in 2048. In a regime where the full-scale is set sensibly, this error is virtually negligible.

Waveform sampling means there is a tendency to underestimate the amplitude. The digitization error is proportional to the sampling interval and the probe frequency. An approximation of this error, assuming that the measured quantity is always a peak in response, can be obtained on a worst case basis as follows:

1. Assume that the response waveform in the vicinity of the peak has the form:

$$A = A_0.\sin(\omega t+\sigma)$$

Where A_0 is the peak amplitude, ω is the probe's (central) angular frequency, t is time and σ is the phase angle.

2. Assume that the peak condition, where $\sin(\omega t+\sigma)=1$, falls exactly between discrete clock times. Thus the peak measurement would be $A= A_0.\sin(\pi/2+\omega.\Delta t)$ where Δt is the sampling interval (1/digitization frequency). For a 5MHz probe and a 50MHz digitization frequency, the maximum undersize would be about 20% of the peak.

Other Quantifiable Errors

The other quantifiable errors in probe and defect specification contributing to the total error in amplitude are summarized in Table 4.

Inspection Parameter	Likely Tolerance	Distribution Type
Unidentified beam angle variation (Error A)	± 3˚ bounded	Top hat based upon an amplitude calculated using CIVA for simple test cases
Unidentified defect skew (Error B)	± 2˚ bounded	Top hat with an amplitude calculated using CIVA for test cases
Beam squint (Error C)	± 2˚ bounded	Top hat with an amplitude calculated using CIVA for test cases
Scan misalignment (Error D)	± 2˚ bounded	Top hat with an amplitude calculated using CIVA for test cases
Unidentified defect tilt (Error E)	± 3˚ bounded	Top hat with an amplitude calculated using CIVA for test cases
Defect depth (Error F)	± 1mm → 1σ*	Gaussian with an amplitude calculated using CIVA for test cases
Calibration error (Error G)	± 3dB → 1σ*	Gaussian amplitude distribution
Digitization errors (Error H)	Amplitude quantization error ignored, because it is likely to be small. Time quantisation error bounded at 20% (see above) Note that this error could be reduced by digitally resampling the waveform at a higher digitization frequency.	Bounded Rayleigh distribution
Coupling Variation (Error I)	± 3dB → 1σ*	Gaussian amplitude distribution
Probe mispositioning	± 1mm → completing bounding.	Top hat

Table 4 Uncertainties contributing to overall amplitude error. The bulk of the amplitude data ranges have been estimated from simple runs of CIVA using small variations in individual parameters. *Note that σ in this table is standard deviation, and not phase angle as stated in 'error due to digitization'

The general method in error calculation is to associate a distribution of error for each of the identified quantities listed above. Then for a single realization of possible errors, a realization of each source error ($A_n..I_n$) according to the distribution function is made and combined as follows:

$Error_n$= Error A_n + Error B_n+……+Error I_n

A large number (typically 10000) of such realizations are made and the statistics of the error distribution are assessed. It is this process which yields an assessment of likely errors.

Note that this approach to establishing credible errors in amplitude measurement is by its nature approximate in that it uses the model under test to establish the variation in amplitude with likely uncertainty in key parameters affecting the response amplitude. Another approximation is that the typical values of parameters have been used, where in fact there would be dependence upon the exact parameters used for the specific case investigated. Despite these limitations, it is still useful to have a view on what would constitute an anticipated error.

Based upon a survey of sensitivity and application of the distribution functions described above using AMEC's error combination calculation, a normally distributed error was obtained. The mean error was found to be close to zero, with some tendency to underestimate amplitude in most cases, and the standard deviation was nearly 6dB. Thus the experimental and modelled results would be expected to be usually within 6dB of one another.

Other Errors

In common with any experiment, not all the error sources which can contribute to the overall accuracy of the measurement are apparent. Of particular relevance in this study are features of targets which cannot be fully known. For example, defects can possess fine structure which may influence response amplitude in a complex manner, and which cannot be revealed without destructive examination.

CIVA Internal Parameters

CIVA has a number of internal parameters which can be set and can potentially affect the model output. It is for instance possible to select either Kirchoff or GTD modelling to describe the scattering process for planar targets, or Kirchoff and SOV for SDH. It is also possible to set a 'quality' parameter. Some testing of the sensitivity of the model output to optional features has been performed. The selection of the interactions in the models was determined by the advice obtained in the CIVA 10 manual. In some cases where responses are obtained that are not specific to the interaction selected i.e. obtaining edge diffracted (tip) signals from Kirchoff (specular) interactions, an explanation of validity is given.

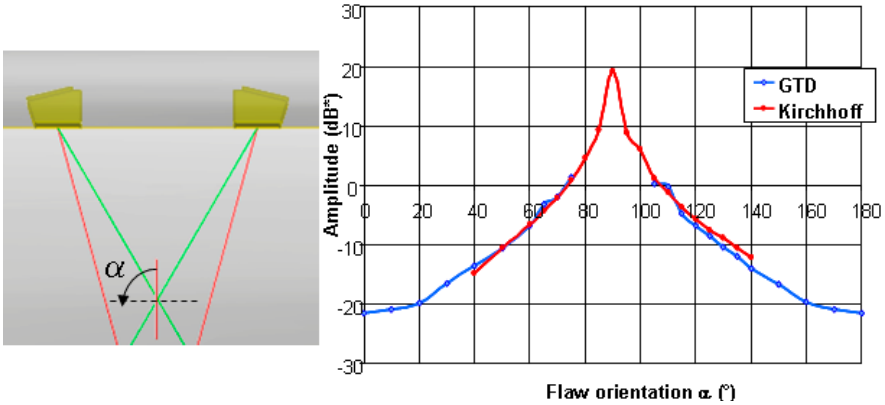

Figure 5 Regions of applicability for Kirchoff and GTD (taken from CIVA 10 manual)

Figure 5 shows where Kirchoff and GTD are applicable in relation to the orientation of the defect, with $\alpha = 0$ representing a vertical flaw. This figure effectively illustrates what is described in chapter 2. The Kirchoff approximation in CIVA gives rise to a tip response that is positioned correctly in terms of time of flight, but the amplitude may be inaccurate, with the error increasing with departure of the scatter direction from specular.

5. Experiments and simulations

Phase 1 experiments

Phase 1 concerned probe modeling and defect response from simple artificial defects and reflectors, such as common reference targets as SDH or notches or mechanical fatigue cracks in parent material. Also some work was done to test the models´ performance with TOFD and phased array applications.

Task 1

Task 1 concerned the collection and modelling of ultrasonic echo data collected from a series of lab-grown high-cycle mechanical fatigue cracks in stainless steel plate samples, referred to as SKI-plates or samples. The manufacturing process would be expected to generate defects which are relatively smooth faced and sharp tipped. These characteristics would tend to make the experimental data a good test of tip signal amplitude, reasonable test of corner response and signal appearance likeness. The cracks in these samples have since their manufacturing proven to be very tight and efforts have been made to increase their width with varying results. An effect of this can be seen in task 3, where signals are seen that wouldn't be present if the defects were ideal.

Samples have been investigated which are 36mm thick with fatigue cracks including through wall extents of 10%, 20% and 50% of the plate thickness. The plates (20% & 50%) are similar to those used in "Experimental Validation of UTDefect, SKI

Report 97:3" [2], but in this case made of stainless steel instead of carbon steel. UTDefect is a simulation software developed at Chalmers University in Gothenburg, Sweden.

SKI Samples
SS 36/3.6
SS 36/7.2
SS 36/18

Table 5 Samples used in Phase 1, task 1

The smallest defect, at 10% through wall extent, corresponds to a size of 3.6mm, which is at the limit of the validity of the models in Kirchoff and GTD. The models are only valid for when the defect extents are significantly greater than the wave-length.

An example of the result is presented in Figure 6 below.

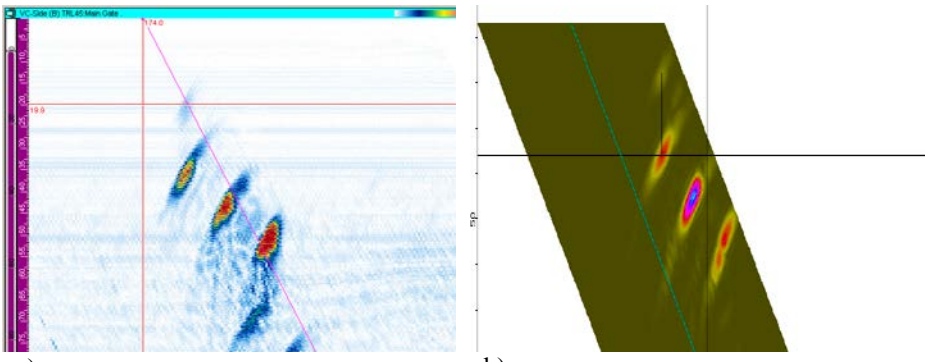

a) b)

Figure 6 45° TRL probe on 18 mm mechanical fatigue crack. a) showing experimental result and b) showing the simulated result. Amplitudes of tip signals within 4dB. Amplitudes of corner signals within 2dB

In the graph (Figure 7) below the distribution of simulated signal responses are shown in relation to the experimentally acquired response. It is important to note that the delta is calculated as follows:

Δ = predicted amplitude - measured amplitude.

The tip responses are separated in respect to simulation method (GTD or Kirchoff).

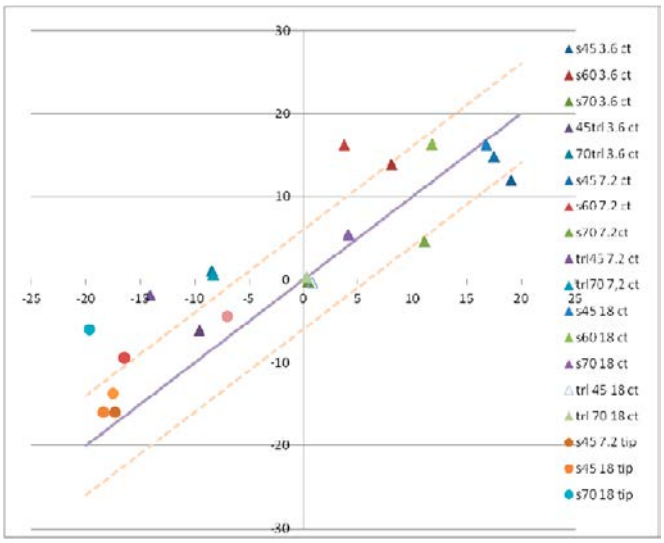

a)

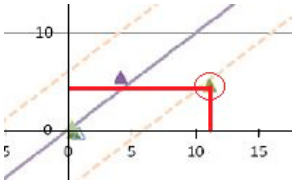

b)

Figure 7 a) Comparison of experimental (horizontal) and CIVA predicted (vertical) amplitude for opposite surface breaking fatigue crack defects of three depths(3,6, 7,2 and 18 mm) insonified with variety of probes. Amplitude data are presented for both crack tips. b) Example of reading the graph. The circled experiment measured +11dB and the corresponding simulation was + 5dB

In the majority of cases, the predictions are within 6dB of the experimental measurements. Largest discrepancies are for the:

- 60° shear corner trap on the 7.2mm defect where the amplitude predicted is significantly larger than was observed in measurement,
- 70° TRL 7.2mm and 3.6mm deep corner traps
- 45° TRL 7.2mm corner trap
- 70° shear tip on 18mm defect

As all experiments didn´t show any tip signals the population in the tip measurements are not as big as for corner trap response. The reason that a significant amount (8 out of 15) tip responses cannot be seen is likely due to the fact that the signal is hidden within the signal from the corner trap or that the diffraction is too weak to be seen. Noise was not modeled in this application.

	Corner trap	Tip (Kirchoff)	Tip (GTD)
Mean delta	+2,6 dB	+7,0 dB	+2,5 dB

Table 6 Mean deviations of amplitudes

Task 2

Task 2, pulse echo examination of reference side drilled holes, concerned data collection from a simple reference block (Figure 8) containing reference holes manufactured from the same material grades and covering the depth range of interest in the SKI samples used in task 1. Again, blocks were scanned with the set of pulse echo probes identified for the project.

The SDH models were processed using Kirchoff and SOV, with the latter taking into account any creeping waves, which would be anticipated for 3mm side drilled holes given the frequency of the probes. Both calculations were conducted to determine how much improvement in the amplitude responses are seen when using SOV.

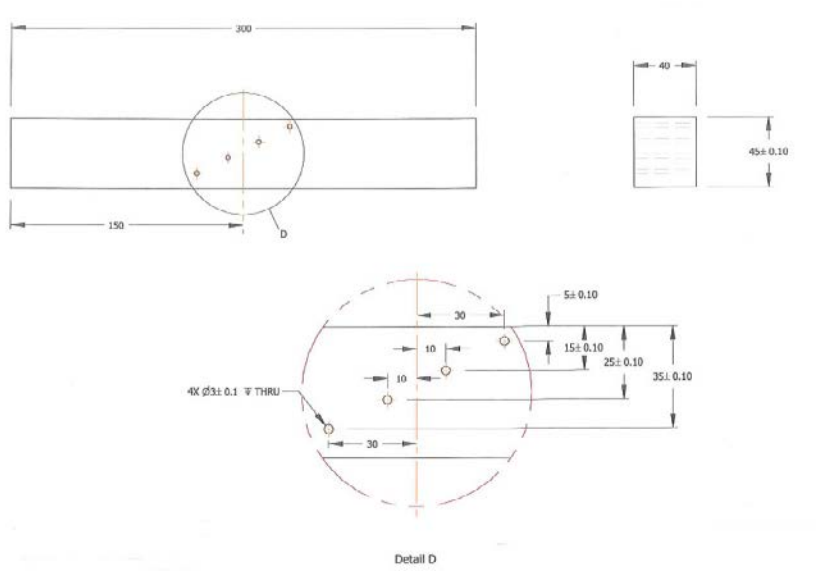

Figure 8 SDH specimen

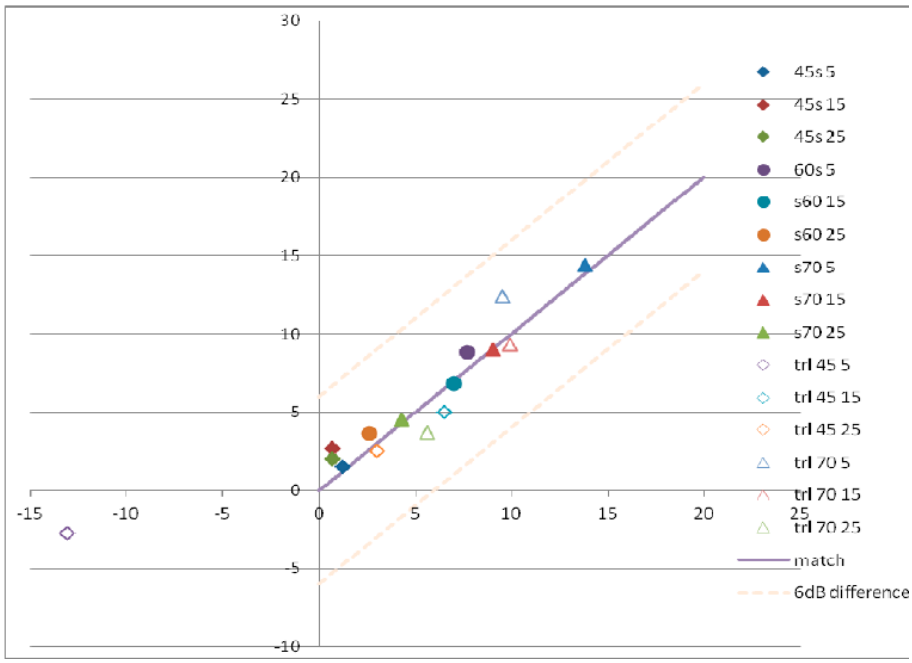

Figure 9 Comparison of experimental (horizontal) and CIVA predicted (vertical) amplitude for three depths of side drilled hole reference targets examined with a range of ultrasonic probes

The differences (delta amplitude) between the measured and predicted echo amplitude sets of results are good for the 5mm, 15mm and 25mm depth SDHs in shear wave mode. Results are also good for the 15mm and 25mm depth SDHs in the compression wave mode. The differences are within 3dB for the CIVA models run using Kirchoff but within 2dB for those run with SOV. However the results for the 5mm depth SDH show less good agreement for the 45° compression wave probe where an amplitude difference of greater than 10dB between measured and predicted peak amplitudes was recorded for both models run in Kirchoff and SOV (the CIVA result overestimated the measured result). This large mismatch would not be unexpected because the hole is at short range, well below the focal range of the probe and in a region likely to be poorly described by the model. Note also that the delta amplitude even for the 70° probe is better than 4dB. The results are presented in Figure 9.

In general terms, the results shows that the response signals for the side drilled holes within the probes' focal range zones are well predicted by CIVA, but that for the shortest beam paths, the mismatch between measurement and CIVA prediction is larger (>10dB peak amplitude error). This indicates that, as might be expected, modelling of scattering for targets outside the probes' focused region is less well matched with measurement than for targets close to or within the focal range of the probes.

These results can be compared to the validation data presented on Extende´s (supplier of the software) web site [4] that presents a similar study. The results compare relatively well. However, the Extende validation data shows even better amplitude estimations from CIVA. The reason for this may be how the test was performed and as the experimental setup is unknown, the results are not directly comparable.

Task 3

The third task dealt with limited application of time of flight scanning to the SKI sample set. To this end, the 50% defect (18mm fatigue crack) was scanned using 30° probes from both sides of the sample as illustrated in Figure 10. To clarify nomenclature, near side scanning refers to scanning from position (A) and the far side from position (B). Near and far is referring to the crack opening.

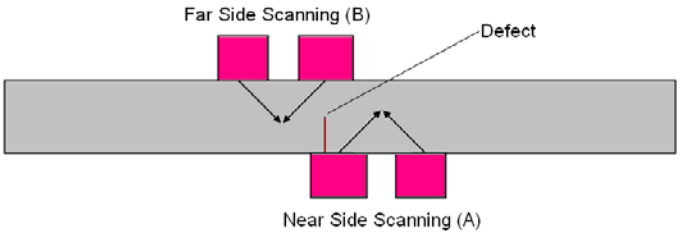

Figure 10 TOFD scanning setup

As amplitude is not of great importance when evaluating TOFD data no analysis of the predicted amplitudes was made. It was noted though that the predicted signal amplitudes are within 4dB of the experimental case. What is important when evaluating TOFD data is the timing of the signals and the phase response of the different echoes and diffraction signals, so these properties has been evaluated.

The comparison that can be made consists of assessment of:

- Relative phasing;
- Arc shape and general appearance;
- Timing;
- Relative amplitude – qualitative.

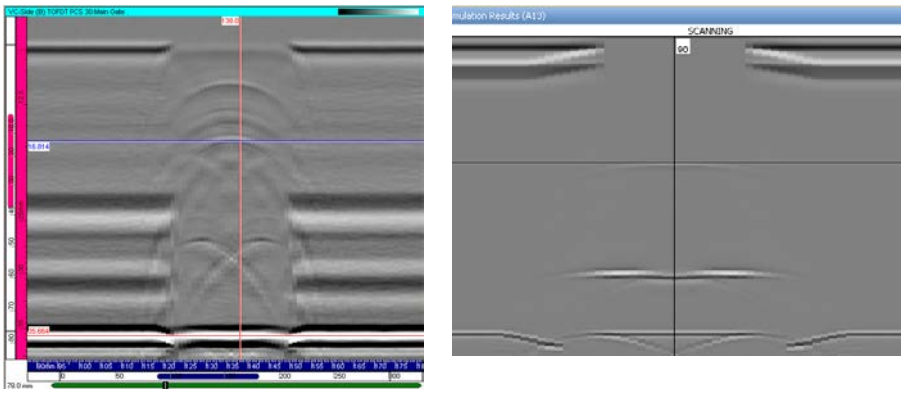

Figure 11 Near side experimental scan and simulation

The results in Figure 11 show the response from the defect from the near side. The main signals' phase relationship in the experiment and model are the same. There is however additional signals in the experimental results not present in the modelled

results. These signals were discussed in chapter “Task 1” where the SKI samples were introduced.

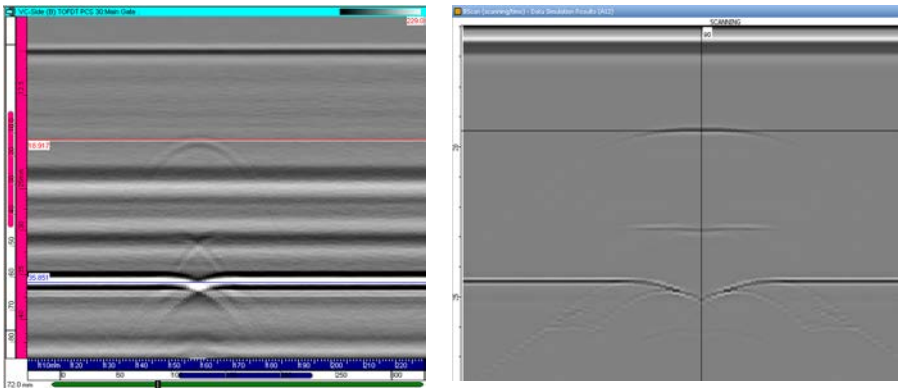

Figure 12 Far side experimental scan and simulation

Generally these signals are secondary to the main features necessary to detect and size the defect. The phase between the lateral wave and back wall appear to have the expected 180° phase difference in both the experiment and CIVA. Where relevant comparisons can be made, for the signals present in both images, the arrival times of the tip signal are very similar in both experiment and CIVA prediction. It is possible to shift the phase of the ultrasonic pulse in CIVA to better match the appearance of the signals of the experiment. This was not done as only the relative phases of the different signals are of interest.

The far side experimental data (Figure 12) do not show the multiple tips found in the near side scans. There are a variety of possible explanations for this ranging from fine structure of the defect through to the relative strength of the diffraction coefficient for the two sets of extreme incidence conditions.

There is TOFD validation data on the suppliers´ web site [4]. It is explained that the CIVA model is not very accurate regarding amplitude with probes that have bandwidths above 80%. This correlates well with our observations. It is important to remember that a high bandwidth is desirable in TOFD applications to ensure as large beam spread a possible.

Task 4

The fourth task compared model and experimental data collected from a series of FBHs when examined with pule echo probes from the probe set.

The comparison between experiment and simulations that can be made consists of assessment of:

- Echo dynamic appearance / pattern recognition
- Amplitude

An example of experiment versus simulation is shown in Figure 13 below. Note that no back wall reflection was simulated and are not present in the simulated B-scan. The simulated B-scan also shows an overlay of the test specimen.

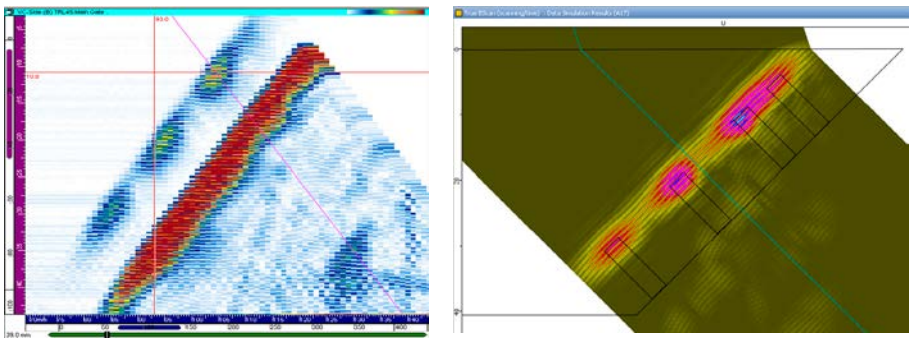

Figure 13 Measured and simulated B-scans for inclined FBH targets

The overlay has given very interesting information, as it has shown that when using higher angle probes, the data seems to be displaced. An example of this is shown in Figure 14 below.

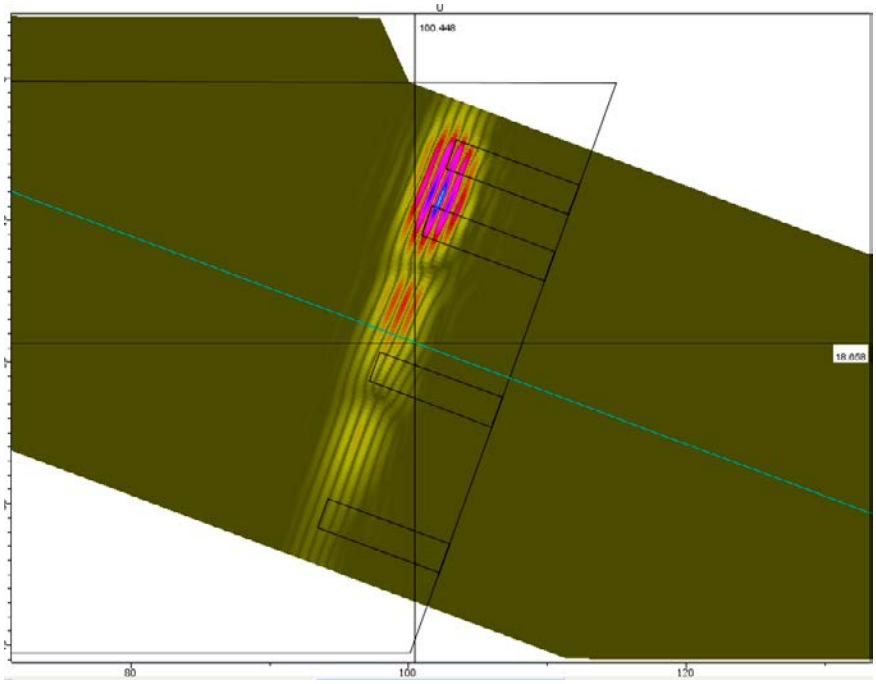

Figure 14 Displacement of Maximum amplitude with depth (70° compression) for FBHs

The displacement of signals is also present if the simulated data from Task 2 is presented with an overlay. See Figure 15.

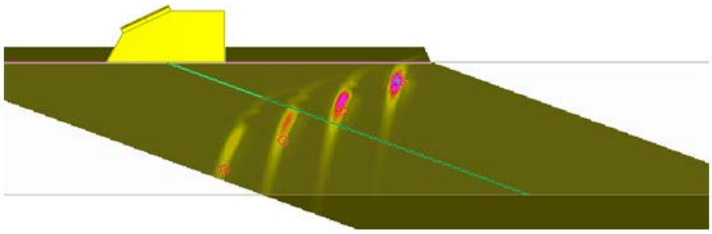

Figure 15 Displacement also present on SDH-data (70° compression)

The reason for this misplacement is not fully investigated.

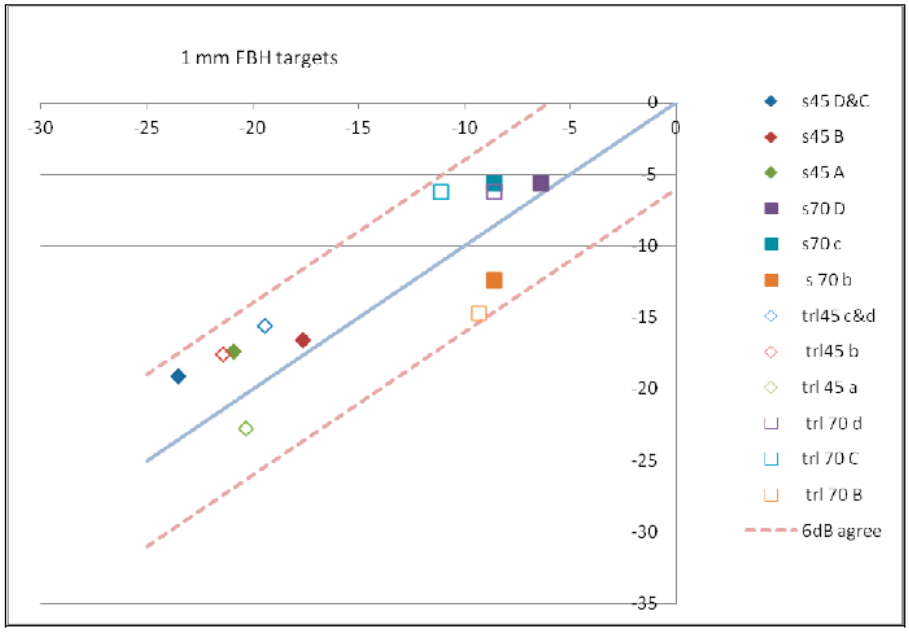

Figure 16 Comparison of experimental (horizontal) and CIVA predicted (vertical) amplitude for 1 mm FBH targets examined with a range of ultrasonic probes

In this case (Figure 16), all predicted responses were within ±6dB. In general the 70° responses were of higher amplitude than the 45° responses.

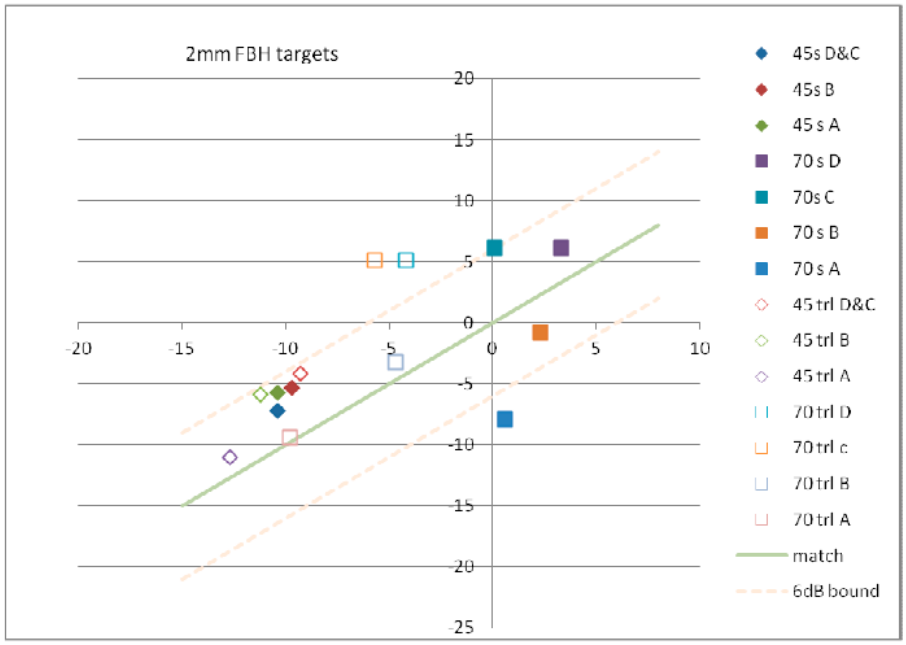

Figure 17 Comparison of experimental (horizontal) and CIVA predicted (vertical) amplitude for 2 mm FBH targets examined with a range of ultrasonic probes

For the bulk of the cases examined (presented in Figure 17), predictions and measurements were within 6dB. Largest differences exist for the 70° TRL probe at short range and the 70° conventional shear wave probe examining the deepest FBH.

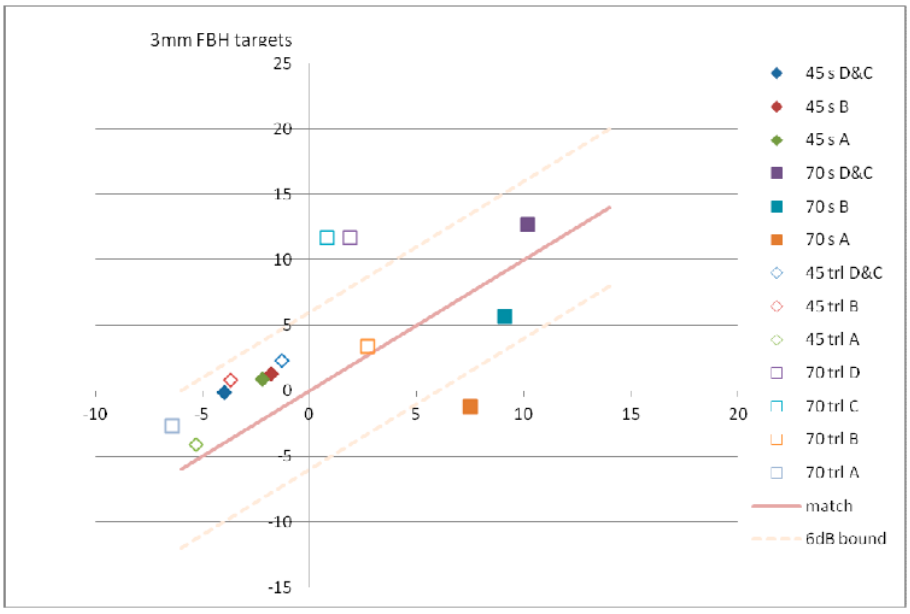

Figure 18 Comparison of experimental (horizontal) and CIVA predicted (vertical) amplitude for 3 mm FBH targets examined with a range of ultrasonic probes

As for the previous plot (Figure 18), the difference between the measured and calculated amplitudes for the majority of cases is within 6dB. As observed in the previous

plot, the largest differences occur for the shallowest holes (C&D) observed with the 70° TRL probe and the deepest hole (A) insonified by the conventional 70° shear wave probe.

Task 5

The fifth task investigated the prediction and experimental data for a range of surface breaking notches with tilt. The test specimens are presented in Figure 19 below. The notches were scanned from both directions, providing a test set with defects with tilts -20°, -10°, 0°, 10° and 20°. The scans were performed so that the notches were far surface breaking.

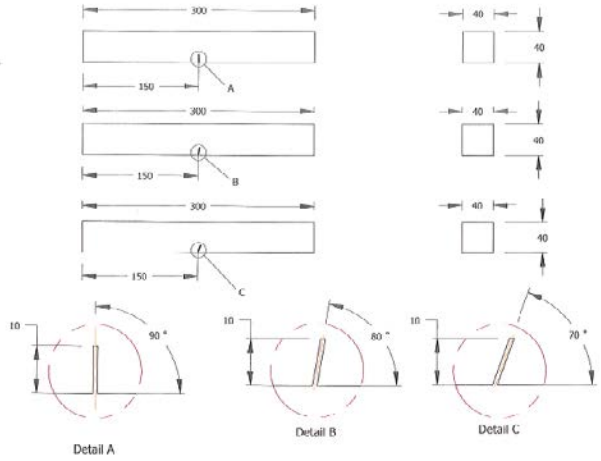

Figure 19 Test specimens task 5

The differences between simulated responses and experimental response amplitude are compiled in Figure 20. The mismatch between measurement and theory is quite large in some cases – in particular at 60˚ beam angle cases. The values in the graph are calculated as simulated amplitude – measured amplitude. The mean delta amplitude value is -3,8dB and the standard deviation comes out quite large at 6,5 dB.

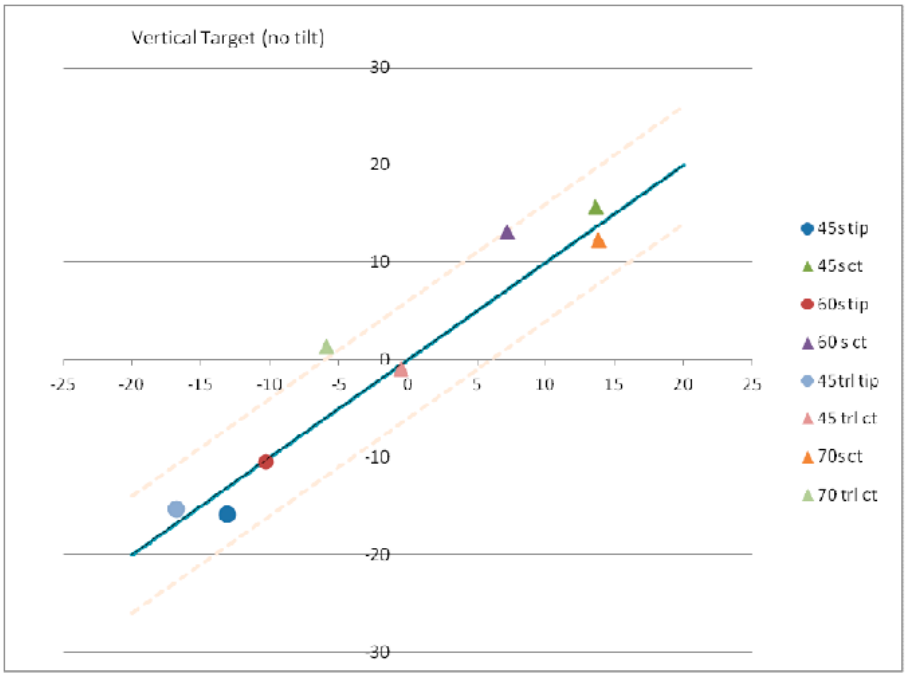

Figure 20 Vertical 10mm slot showing tip and corner trap response for a variety of probes

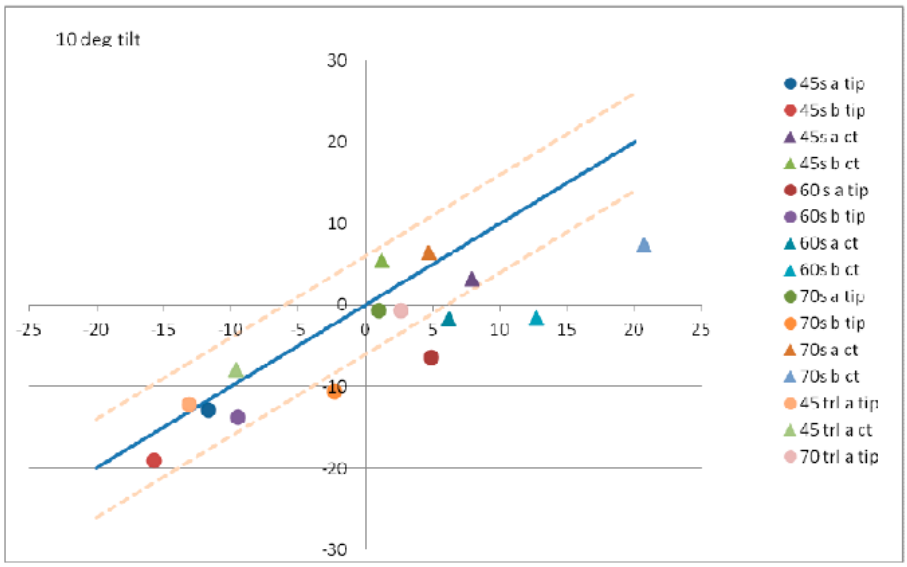

Figure 21 10° inclined 10mm slot showing tip and corner trap responses for a variety of probes. The spread of results is larger than for a vertical slot. The CIVA model tends to under estimate the echo amplitude in these cases

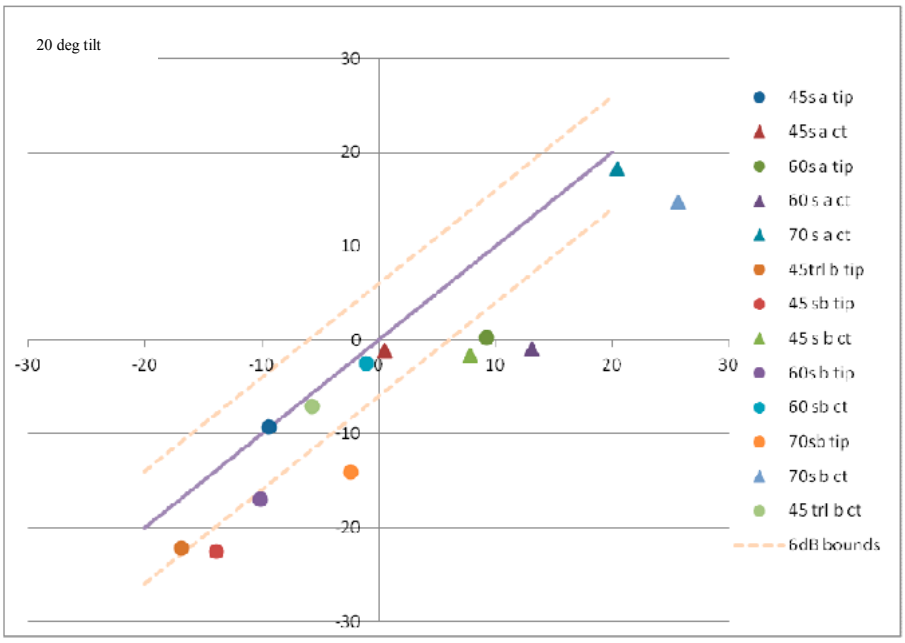

Figure 22 20° inclined 10mm slot showing tip and corner trap responses for a variety of probes. Once again, the spread of results is larger than for the vertical case. The CIVA model tends to underestimate the echo amplitude where there is more significant error

Task 6

The sixth task investigated inspection of embedded planar defects with various configurations which are of interest for fabrication targets. Comparative results were only made between the first three sets of defects shown in Figure 23.

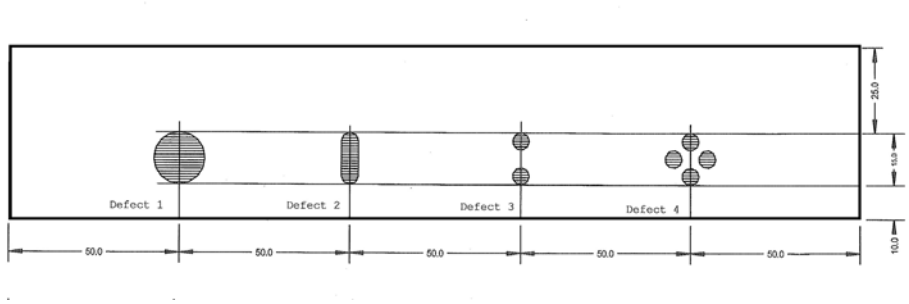

Figure 23 End view of embedded defects used in task 6

Below an example (Figure 24) of the signal response from defect 1 is shown when scanned with a 45°SWK probe.

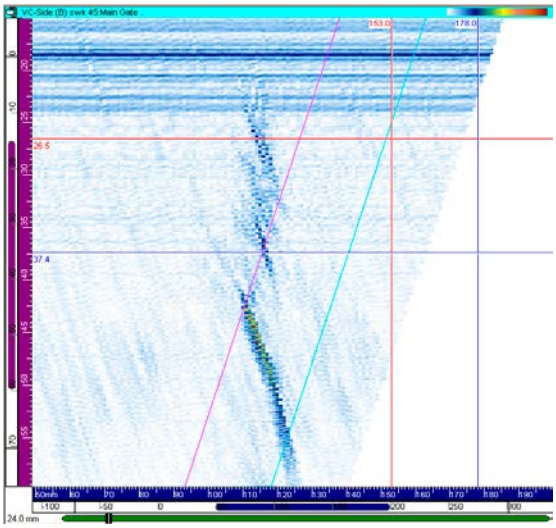

Figure 24 Defect 1 experimental signal response

The experimental results showed that the upper tip signals for the shear wave probes have a smaller amplitude than the lower tip signals for both defects 1 and 2. The predicted responses show a high level of deviation from experimental observation for the higher angle probes. Response predictions from the UK Nuclear Utility simulation model PEDGE (UT simulation software) are included. The predictions made using this model are poorly matched with experiment too. It is suspected that much of the result here is linked to issues with the defect's final form.

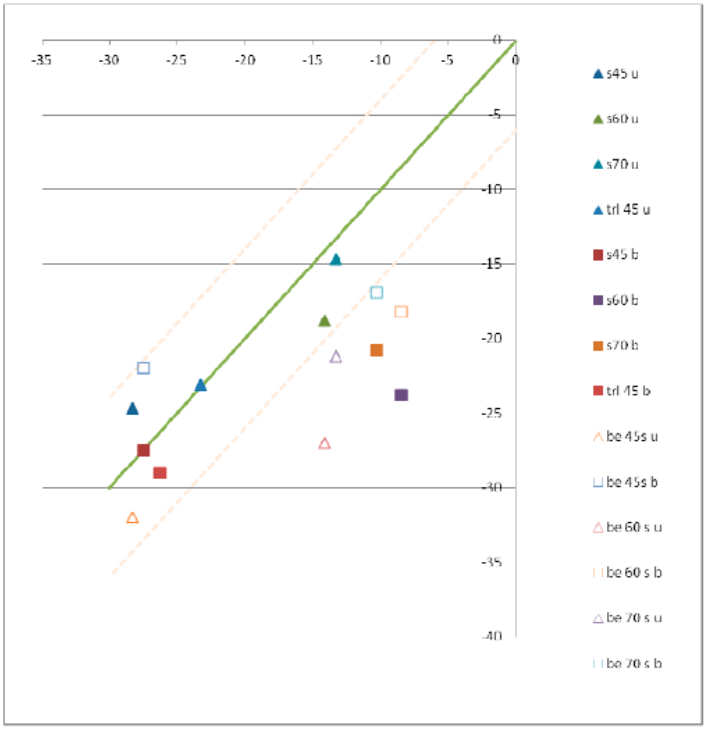

Figure 25 Comparison of experimental (horizontal) and CIVA predicted (vertical) amplitude for a circular vertical HIP´d target examined with a range of ultrasonic probes. Echoes are associated with the target tips labelled 'u' upper and 'b' bottom. Hollow triangles and boxes are run with UK model PEDGE

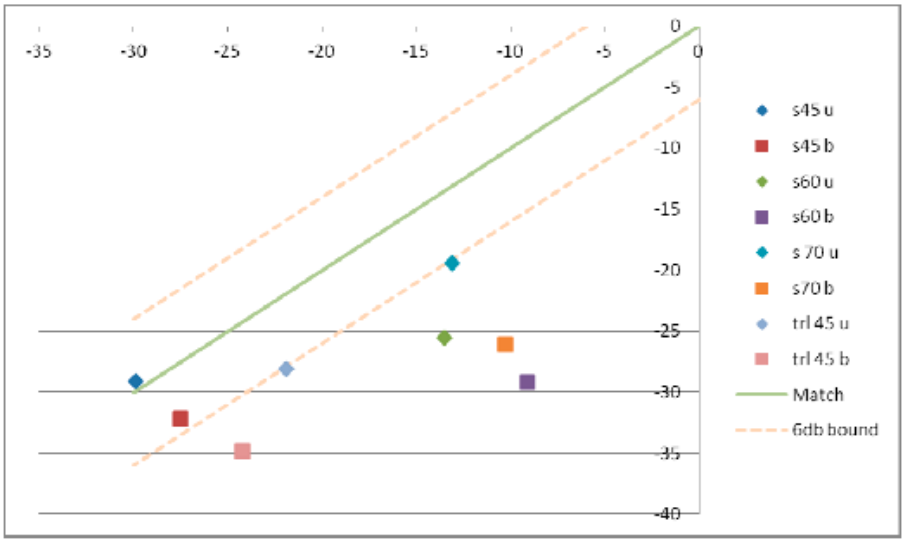

Figure 26 Comparison of experimental (horizontal) and CIVA predicted (vertical) amplitude for an elliptical vertical HIP'd finns i listan redantarget examined with a range of ultrasonic probes. Echoes are associated with the target tips labelled 'u' upper and 'b' bottom

Task 7

In the seventh task, a 64 element phased array with a center frequency of 5MHz was used to investigate the basic phased array modelling capabilities within CIVA. The data collection activity was performed at AMEC using a Peak NDE Microplus 5 PA system.

In summary, two samples from the reference set were used in the investigation:

- Reference block containing 3mm reference holes at depths of 5, 15, 25 and 35mm from the surface;
- 10mm vertical notch sample (as used in task 5).

The reasons for using these two samples were that:

- the samples are relatively simple and both their form and the reflectors they contain are well defined,
- they provide a ready means for checking relevant beam-forming prediction capability, and
- the results correlate well with the modelling and experimental data collection programme undertaken in the earlier stages of the project.

The Peak NDE Microplus 5 PA system is equipped with a delay law calculation tool (Arraygen), which produces delay laws in a file based form which can be imported into Microplus to configure the probe's firing.

The delay law calculations were exported from Arraygen as a .MPS files and CIVA as .law files. For both sets of delay laws the figures produced were the same, or rather, the delay between each of the elements are identical. CIVA does appear to apply an offset at each angle of the sector scan but this has no effect on the delays between each element.

Table 7 shows the results from the corner trap and tip of the vertical notch. The 10mm vertical notch sample block (as used in task 5) was scanned experimentally from both sides (of the defect) and a mild asymmetry in results was observed which could arise from slight irregularities on the target or a small inclination or tilt angle. Options within CIVA have been used to select either the Kirchoff (default) or GTD tip response algorithms.

The amplitudes are reported with reference to a 3mm SDH at a depth of 40mm. The results show that there is less than 1dB difference between the experimental results for the corner tap response when scanned from two sides. Overall the modelled result is within 1.5dB of the experimental results. Figure 27 shows the experimental and modelled results as a B-scan image. In both sets of results the tip and corner signals can be clearly distinguished.

	Experimental – Side A	Experimental – Side B	CIVA	
			Kirchoff	GTD
Corner Trap	-0,7 dB	-0,1 dB	0,5 dB	N/A
Tip Signal	-6,0 dB	-7,8 dB	-17 dB	-20 dB

Table 7 Corner trap and tip responses from vertical notch

The tip signal amplitudes obtained from the experimental and modelled results show a larger difference than the corresponding corner response results (Table 7). The GTD model gives the lowest amplitude and this is more than 12dB lower than the amplitude obtained experimentally from side A. This result is probably explained by the slot having a relatively large width which acts as a reflector, whereas in the model the notch was represented by a slot with minimal width, which would give a lower amplitude response compared to a diffracted tip response.

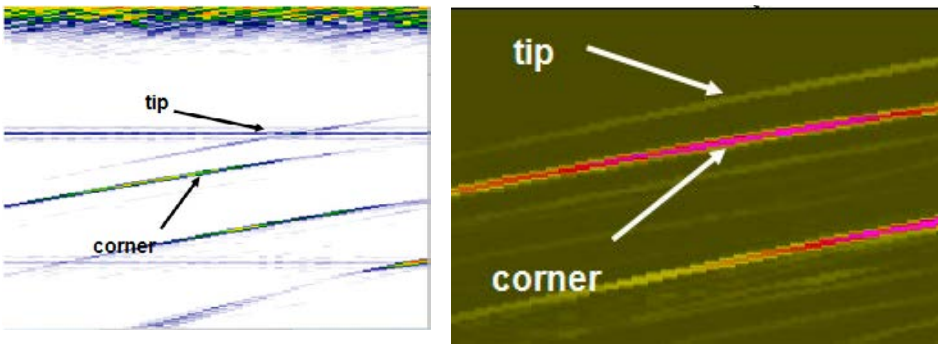

a) b)

Figure 27 B-scan images of the response from a vertical notch. a) showing experiment and b) showing simulation

The results from the reference hole calibrations are given in Table 8. The amplitude response differences between the modelled and experimental results are within 1dB for the hole at a depth of 15mm and within 1.5dB for the reference hole at 35mm. The calibration reference used in this configuration was a 3mm SDH at a depth of 25mm. The amplitude differences relative to the reference hole are small because of the unfocussed beam configuration however this is the case in the modelled and

experimental results. The 5mm hole could not be scanned experimentally due to its proximity to the surface; hence no results are presented for this case.

Hole Depth	Experiment	CIVA
15 mm	1,3 dB	0,3 dB
35 mm	-1,5 dB	-0,1 dB

Table 8 Amplitude response from reference holes

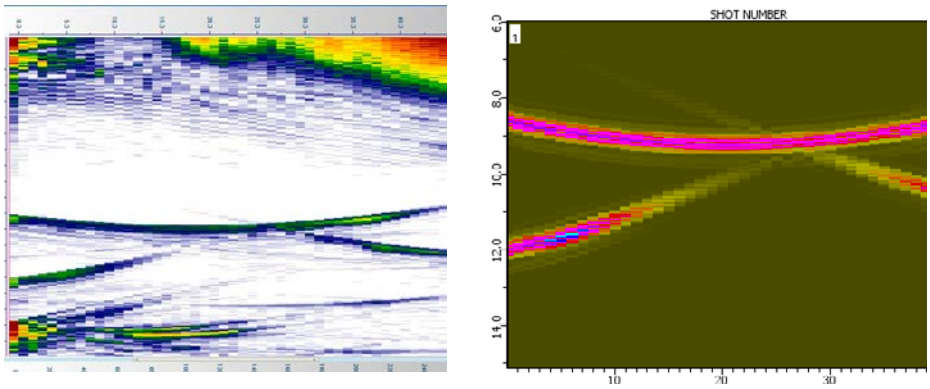

a) b)

Figure 28 B-scan images from a 0-45° sectorial scan of a 25 mm depth 3 mm SDH. a) showing experiment and b) showing simulation

The results from the phased array experiments has been in accordance with what has been seen in the other tasks, specular reflection and corner traps are modeled with good precision, but tip diffraction is usually not as accurate. As discussed above, this may be due to the differences in model and samples as well as less accurate model predictions.

Conclusions Phase 1

The trials performed in phase 1 largely resemble typical methods for calibration in qualified procedures. The specific UT methods (PE, PA and TOFD) assessed are also common in qualified inspection procedures.

As simulated amplitude response, phase and delay laws match the experimental results well this is a solid foundation to base more advanced simulations on.

Phase 2 experiments

Phase 2 handles complex geometries in simple (homogeneous and isotropic) materials. A set of test samples has been identified to contain a relevant set of geometries and reflectors. However, in some cases full knowledge of the manufacturing of the sample has not been known.

Task 1

The sample identified for task 1 is a forged alloy 403 reduction with three notches as shown in Figure 29.

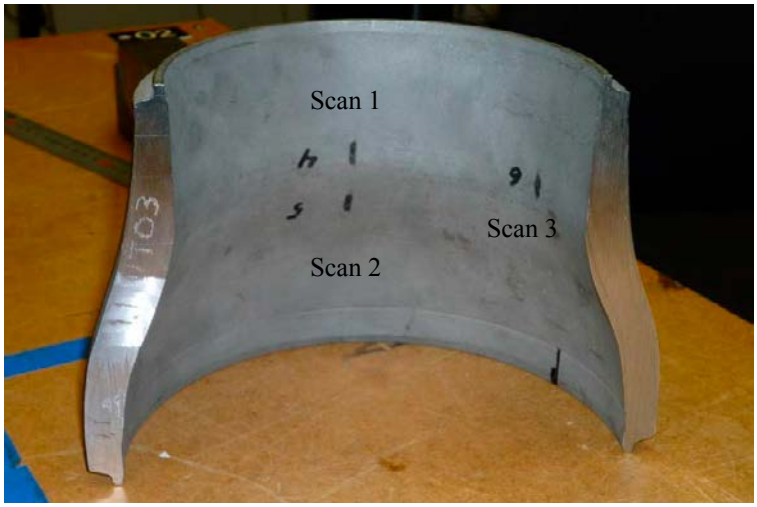

Figure 29 Specimen 1.1_UT03

All available experimental scans of the complex geometry Specimen 1.1_UT03 (Figure 29) have been modelled. All scans have been modelled as half-skip considering both longitudinal and transverse (shear) components and mode conversion.

Initial studies made using CIVA 10 were incorrectly configured without a back wall, which meant skipped responses were not modelled as intended. When runs were repeated using CIVA 11, a warning was generated which enabled the fault to be rectified. Examples of B-scan results are shown in Figure 30.

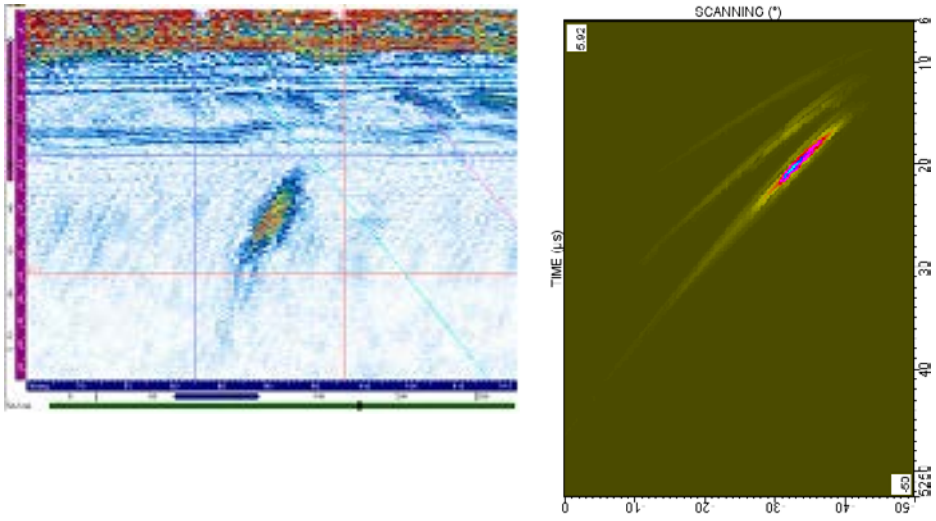

a) Experimental measurement b) CIVA 11 prediction

Figure 30 Comparison of experimental measurement (a) and CIVA prediction (b) in B-scan display. CIVA prediction made using CIVA 11

The shape and appearance of the shear signal from Defect 1 in the specimen (3rd response peak from left in the CIVA prediction (Figure 30) is similar in the CIVA and experimental data. Two earlier echoes are apparent in the CIVA prediction, which arise from:

- compression wave
- mode converted compression/shear wave or vice versa

and are significantly lower amplitude than the shear signal. These faster routes are credibly lost in the noise in the experimental response data.

For the shear reflection, the amplitude match is fair as shown in the following table. The CIVA prediction consistently underestimates the measured signal by a little over 6dB in each case.

Target and scan orientation	Peak Amplitude [dB] for shear component from corner	
	Measured	CIVA
Defect 1, MWB 45 measured in one direction and then the other	-12,3 & -9,2	-16
Defect 1, MWB 60 measured in one direction and then the other	-19,6 & -17,7	-25,8

Table 9 Tabulated results

Task 2

Task 2 handles relatively small convex radius and reflections from a series of SDH´s. The sample also contains a weld, but it has not been modeled within this phase, as it would fall under phase 3 (difficult materials). Figure 31 shows the sample (NDT545, Ø135 mm) and the three different scans that were made (including through weld inspection).

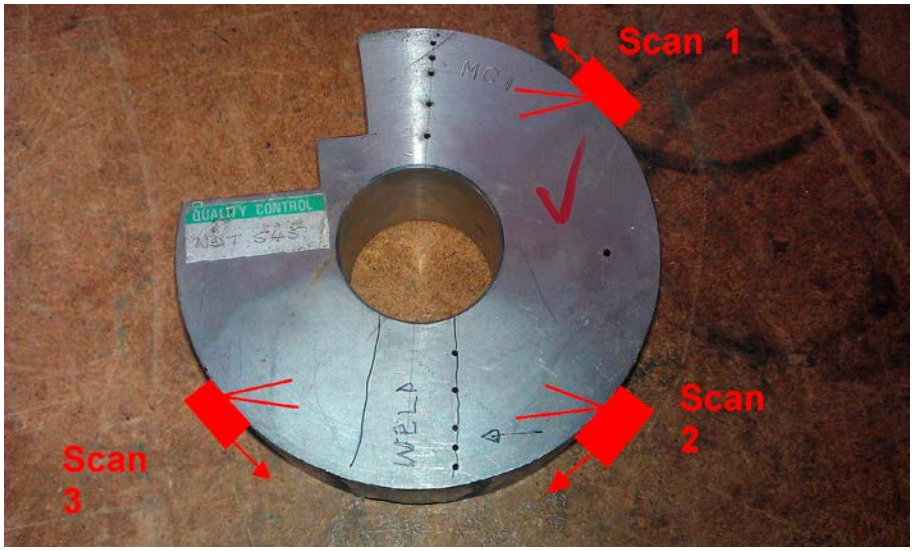

Figure 31 Phase 2 task 2 sample and experimental scans

The maximum amplitude for each SDH was recorded together with -6dB half widths to describe the signal response in quantitive terms in order to establish comparable results between experiment and simulations. Two runs of simulations were carried out on each scan. One with Kirchoff and one SOV. Also the SOV-run was run with slightly different lengths of the probe wedge, as it during the work was discovered that the measurements were a little of at the time of the first run.

Aside from the differences in probe wedge diameters, the obvious difference between the Kirchoff and SOV simulations is that the SOV clearly displays the Rayleigh waves that appear behind the reflection signals.

The simulated results (Kirchoff and SOV) are presented in Figure 32.

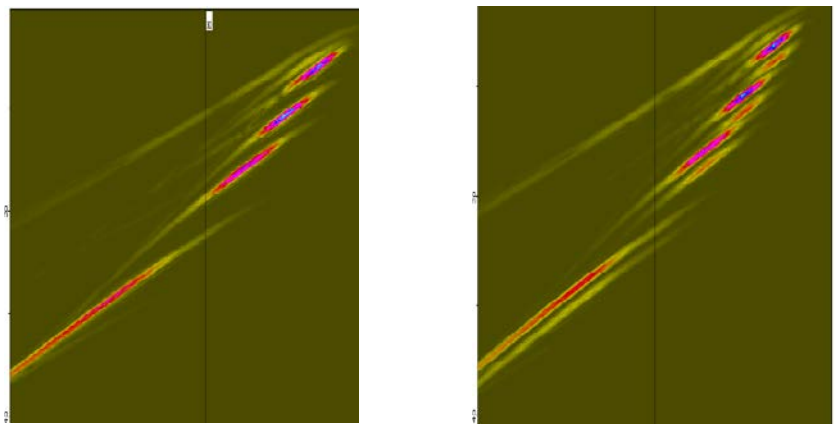

a) b)

Figure 32 Simulated B-scans, a) showing Kirchoff modelling and b) showing SOV modelling

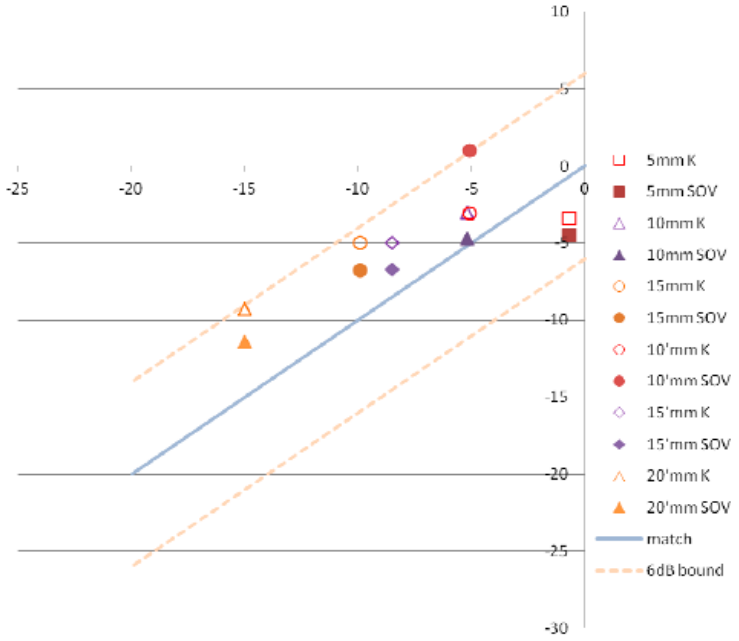

Figure 33 Comparison of CIVA prediction with experimental measurement of echo amplitudes from SDH in the NDT545 specimen. The plot combines scans 1 and 2 whose points are marked with a prime (')

The -6 dB half widths have been measured to produce a comparable metric on the signal pattern appearance. The noise level and attenuation has a large impact on these measurements. As no specific attenuation was modelled in these runs, some additional difference between experiments and simulation may be present that could have been avoided if the material attenuation were also modeled. See Figure 34.

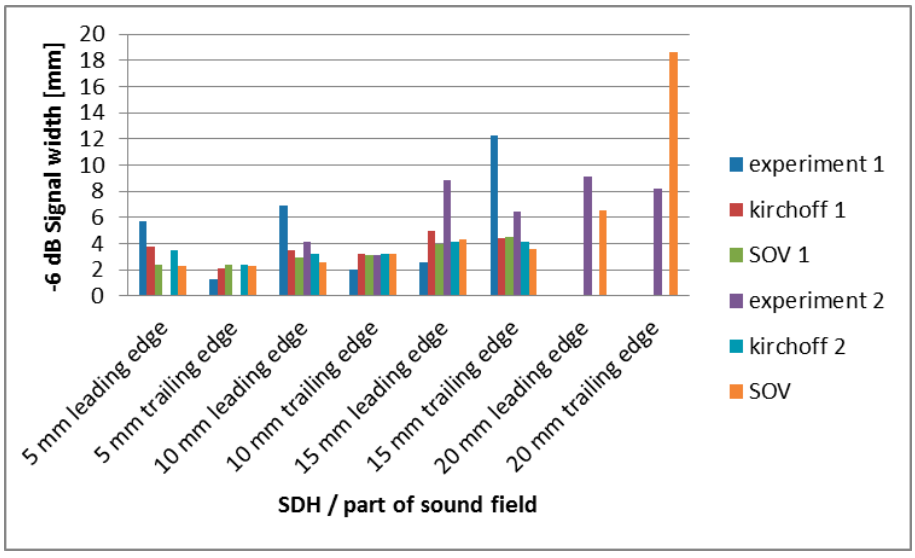

Figure 34 -6 dB half widths

Task 3

Task 3 is similar to task 2 with a similar test specimen but with a little larger diameter (NDT547, Ø163 mm). The third scan, through the weld, was not modelled for this specimen either, as in task 2.

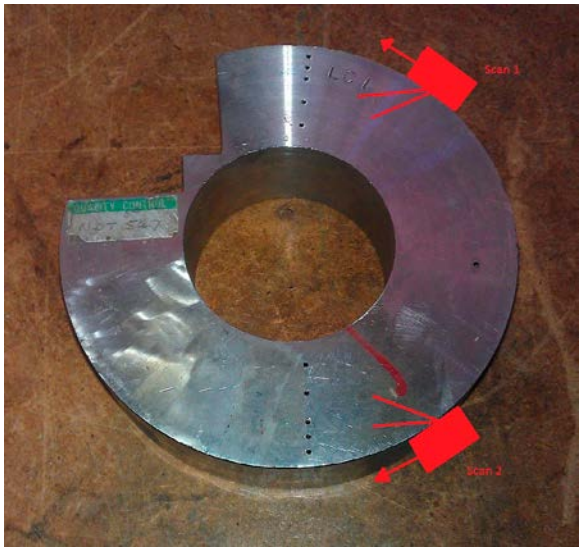

Figure 35 Phase 2 task 3 sample and experimental scans

The simulated scans look similar to those in Figure 32 a and b. The simulations overestimate the echoes systematically to a greater scale on this specimen compared to the one in task 2. Also, the -6 dB half widths are narrower, indicating that less divergent sound field is simulated than what is really the case, see Figure 36. This is also seen in task 2.

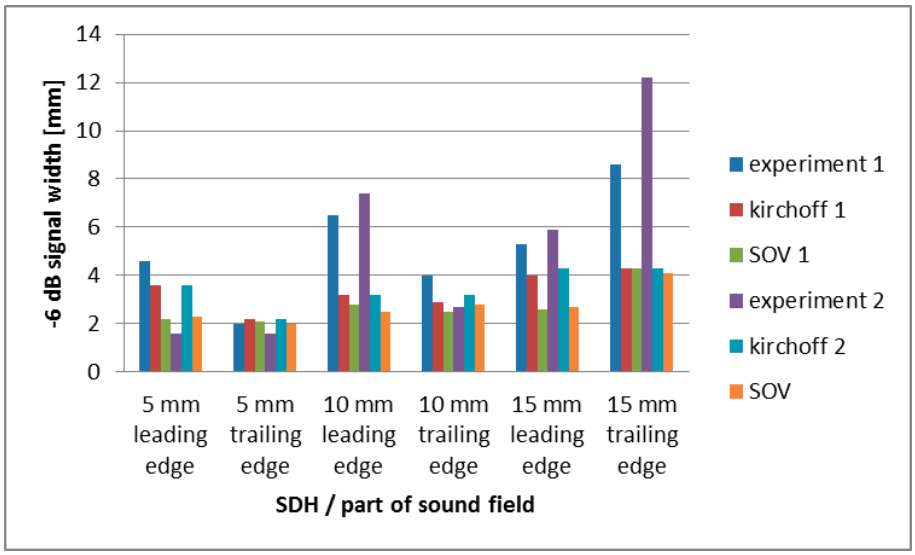

Figure 36 -6 dB half widths

Task 4

Task 4 handles relatively small radius concave geometries. Issues that can arise in this type of applications are poor sonic coupling and lift off. The sample that was used had two different radii and SDH´s on two different depths, see Figure 37. The back wall reflection from the opposite radius has been used as reference to scale the amplitudes.

The scans were rerun similar to task 2 and 3.

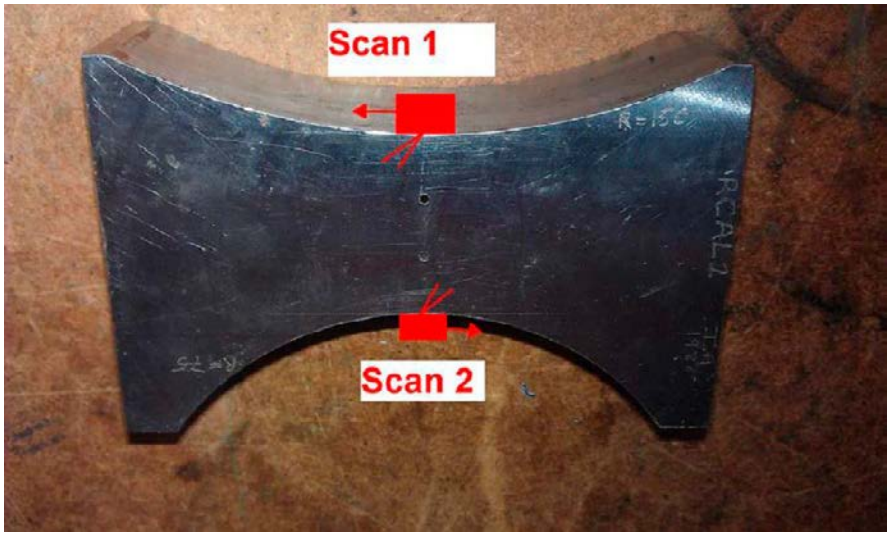

Figure 37 Task 4 specimen and collected scans

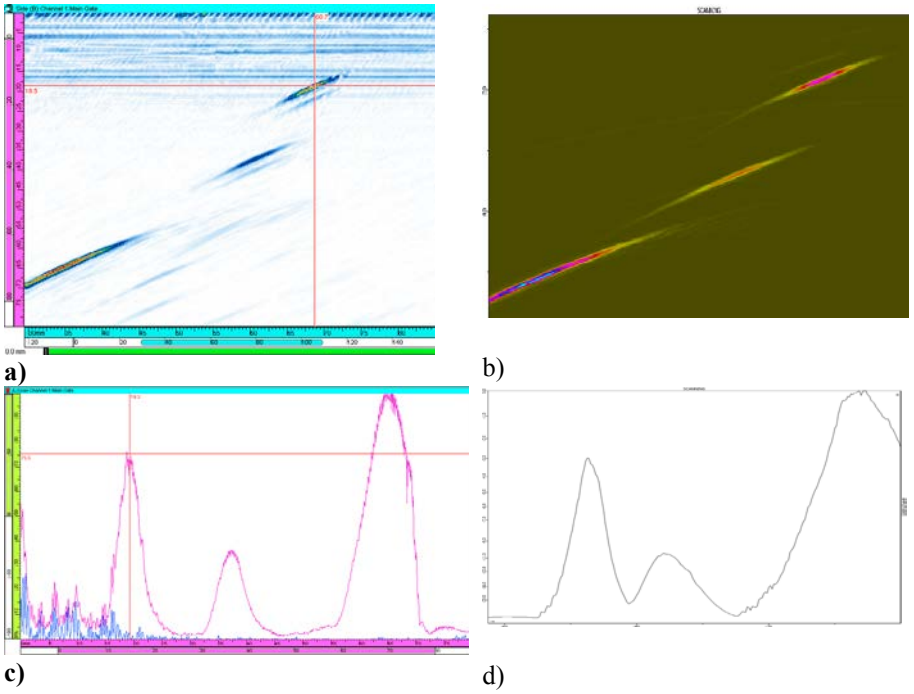

Figure 38 Experimental and simulated scan 1 (a & b), experimental and simulated echo dynamic from scan 1 (c & d)

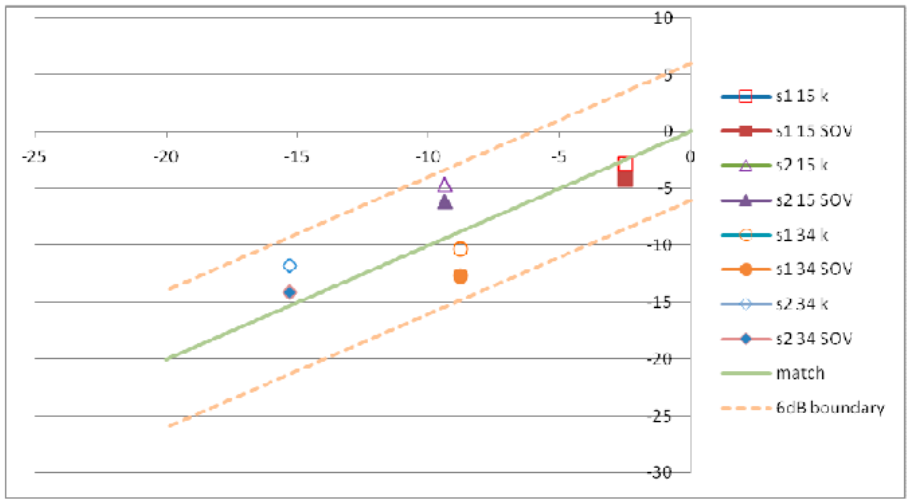

Figure 39 Composite results from scan 1 & 2

The amplitudes are typically within 4 dB. Amplitudes are systematically underestimated for simulations of scan 1, which has a larger radius than Scan 2. The Scan 2 simulations on the other hand tend to overestimate the amplitudes.

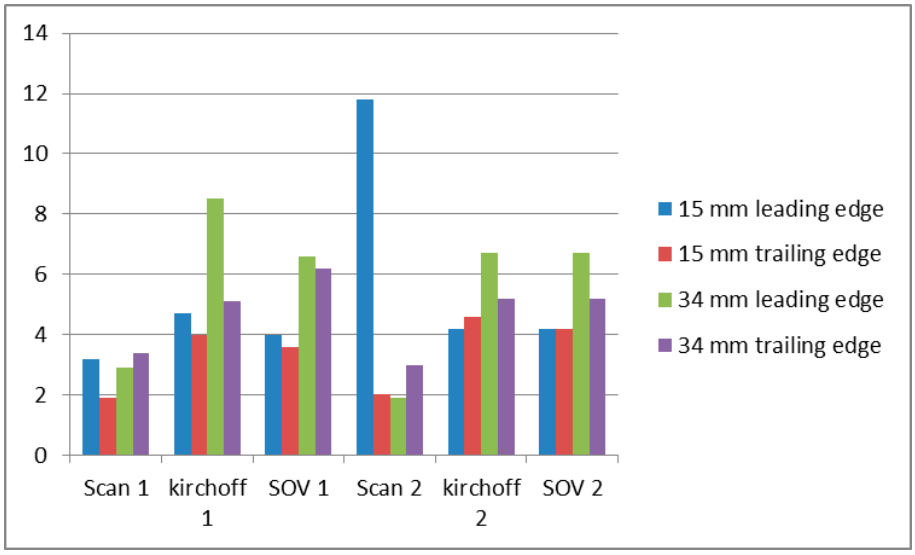

Figure 40 -6 dB half widths

The -6dB half widths in this task are generally larger in the simulations than the experimental values. This is the opposite result from tasks 2 and 3.

Task 5

Task 5 handles somewhat larger radii than the previous tasks, both convex and concave.

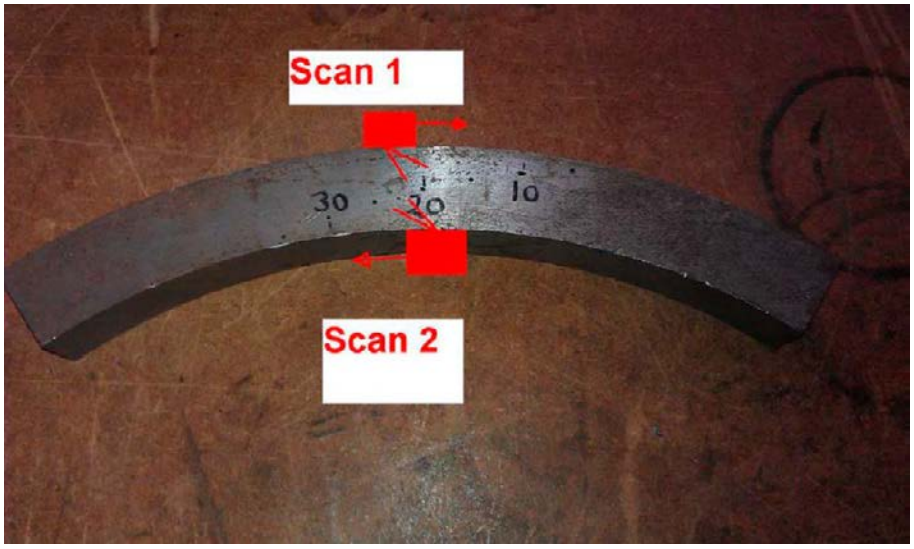

Figure 41 Scans and sample for task 5

The signal response was measured and compared in the same manner as in tasks 2-4.

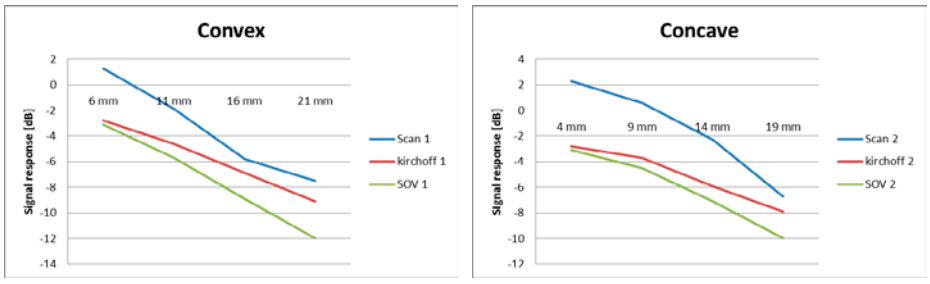

(a) (b)

Figure 42 SDH response amplitude from Scan 1 (a) and Scan 2 (b)

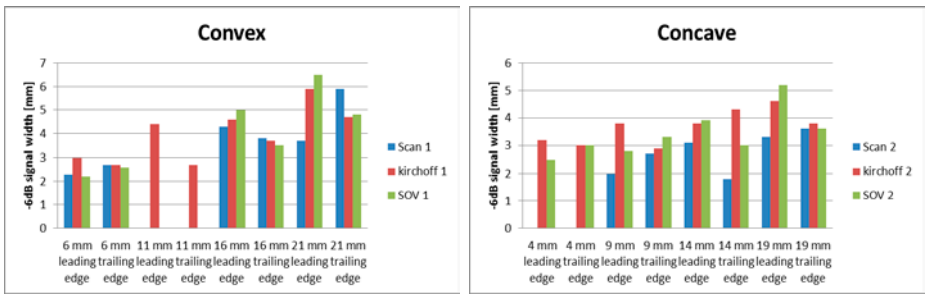

(a) (b)

Figure 43 -6dB half widths for Scan 1 (a) and Scan 2 (b)

Conclusions Phase 2

The aim of phase 2 was to examine how well CIVA handles geometries likely to appear in an inspection situation in a nuclear power plant. During phase 2 more attention was paid to the appearance of the signal pattern in addition to amplitude as in phase 1.

The response patterns predicted by CIVA matches the experimental well although the results from tasks 2, 3 ,4 and 5 suggests that the beam widths are overestimated on concave objects. Relative amplitudes between targets are also well predicted.

Phase 3 experiments

Phase 3 handles the CIVA code´s ability to simulate the impact of difficult materials such as inconel and austenitic welds.

Task 1

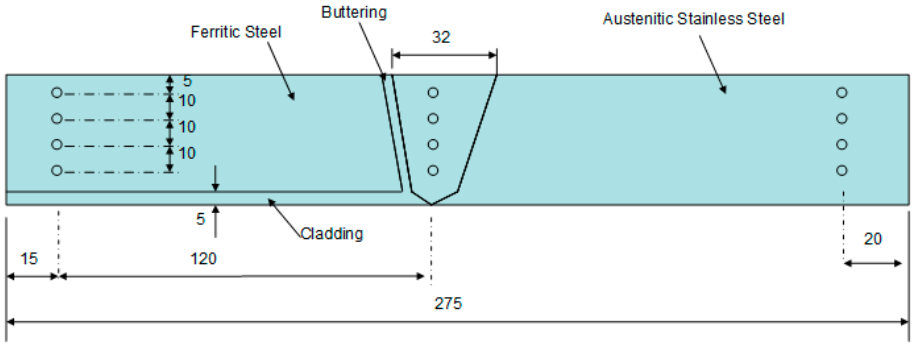

Figure 44 Side view schematic of dissimilar metal weld sample used in experimental study. The stainless steel plate is 316L alloy, and weld material 316

The sample contains a multi-pass austenitic stainless steel weld in a dissimilar metal weld. An etched through section of a similar weld is shown in Figure 45 below.

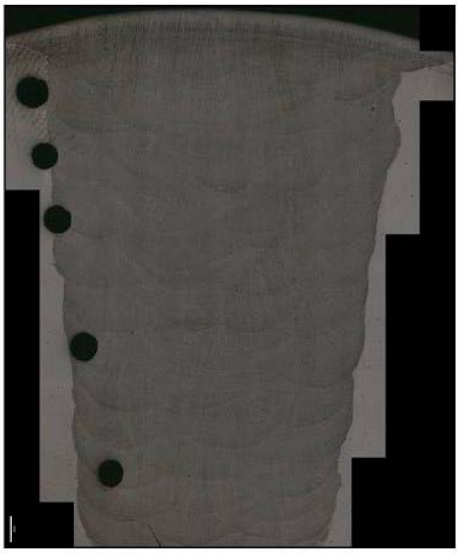

Figure 45 Multi pass austenitic stainless steel weld

This study was inconclusive to some extent because the specimen exhibited few of the effects observed in textured weld inspection. The main reason for this is likely to that the material itself exhibited a low level of anisotropy despite being visibly textured. A further attempt to generate response data for a practical inspection case - the ring samples (NDT 545 and NDT 547 – as seen in Phase 2 and Figure 45 above) which were used to investigate the influence of convex curvature. The rings contained an austenitic weld with a series of SDHs alongside it. The holes were inspected from the parent material (scan 2 in previous study), but in this case (through weld) the beam distortion/attenuation effects were marked in these samples, and the choice of suitable probes limited owing to the extreme curvature, that no meaningful data could be obtained. Trials with immersion technique were made, but without any useful results.

Task 2

A final effort was made in this area by making a specially designed, planar, exaggerated wide v-butt weld test piece, shown in Figure 46. This specimen has been constructed for this cause and extensively inspected using commonly applied probes.

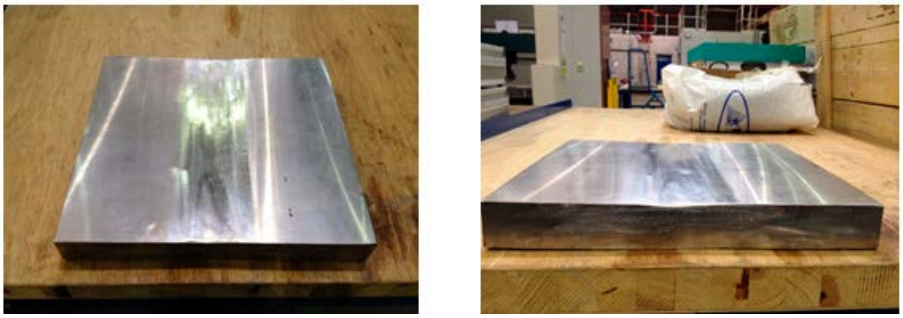

Figure 46 Fabricated textured weld sample with an exaggerated v-butt design and containing a range of slots and holes

The sample exhibited beam bending affects as anticipated and it has been possible to obtain echo data from the reference targets. Difficulties were encountered in generating a full grain table (a graphical representation of the grain structure) for the sample and instead an approximate grain table was used in the modelling exercise that accompanied this work. The grain table has been obtained and digitized as is shown in the following figure (47).

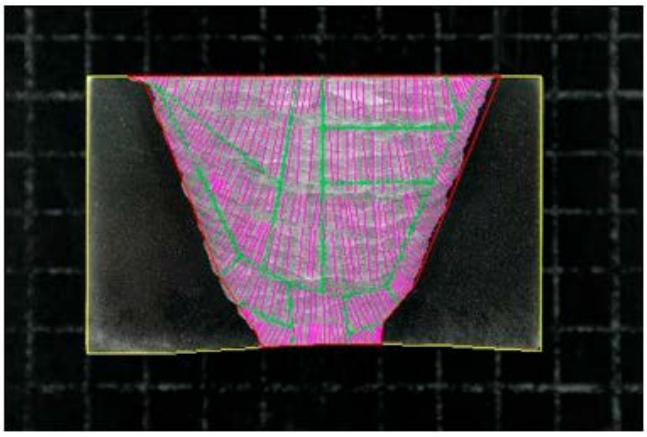

Figure 47 Grain table from AMEC constructed sample. The grain table has been measured using microscopic techniques and a set of lines describing the grain has been marked on to the figure

Results of scanning show that some of the targets were too small to be resolved by all the inspections. In general terms, most of the SDH targets could be detected, but echo data were clearly subject to beam bending effects. This grain table shown in Figure 47 was used to construct models in CIVA. The assumption has been made that the grains lie in the sample plane as the weld section (as in Figure 47) – that the weld is transversely isotropic. In fact this is likely to be a fair approximation. The elasticity moduli in the stiffness matrix was identified through a literature study and chosen as a best estimate. The stiffness matrix for a transversely isotropic material is defined as shown in Figure 48 below. Please note that the values in the picture are just an example, and not necessarily the values used in the actual simulation.

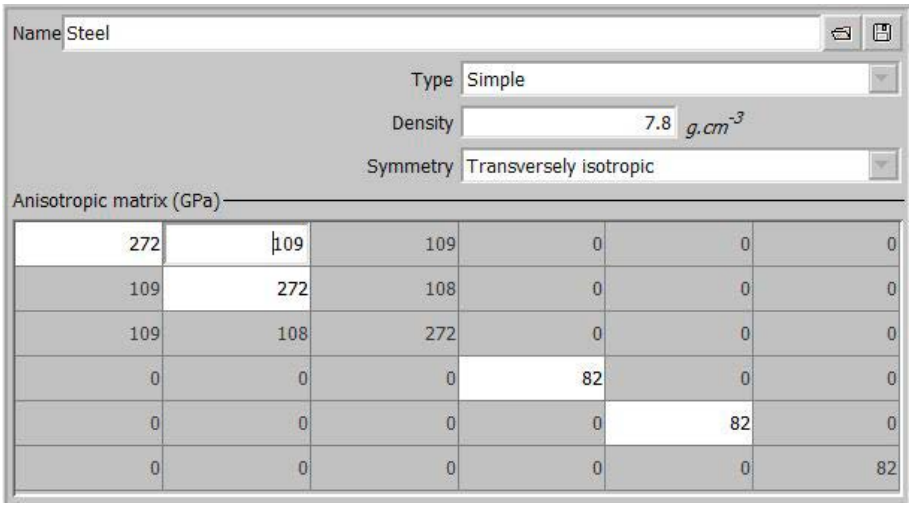

Figure 48 Definition of transverse isotropic material

There tends to be a modest grain slope out of the plane known as the layback angle. The inspections were performed using 45°, 60°and 70° TRL probes with the following essential parameters.

45° TRL 2 focal depth ~25 mm

- Beam angle 48.2°

60° TRL 2 focal depth ~30 mm

- Beam angle 58.4°

70° TRL 2 focal depth ~35 mm

- Beam angle 70.4°

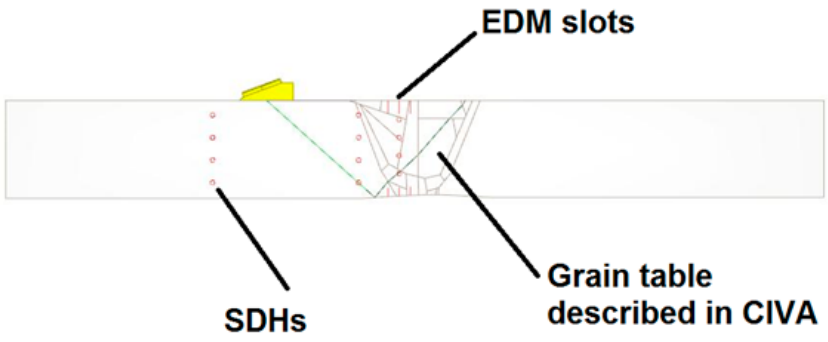

Figure 49 Austenitic weld sample as modeled in CIVA. Note the three sets of SDH targets and EDM slots and grain table

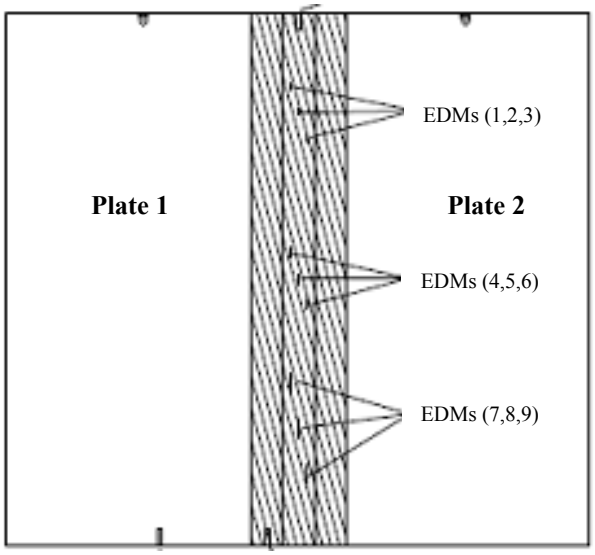

a)

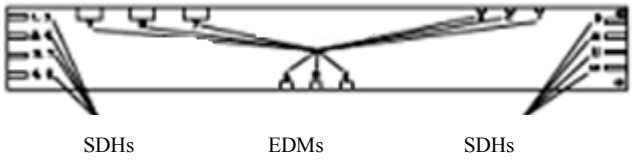

b)

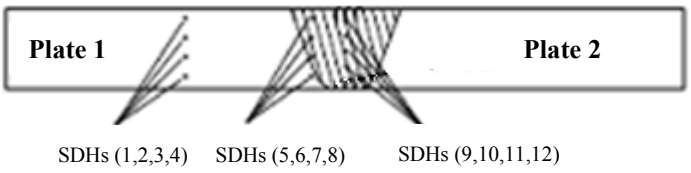

c)

Figure 50 Austenitic weld sample showing the numbering system used which is referred to in the following text. a) top view, b) side view and c) end view

The following figures shows experimental data collected from SDH targets in the weld compared to CIVA predictions. These data were collected with the 45° probe. Figure 50 displays a drawing of the specimen.

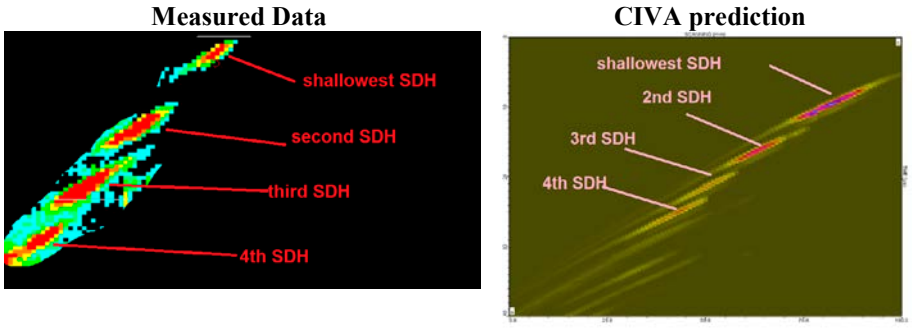

a) b)

Figure 51 Austenitic weld sample plotted in a b-scan, a) inspection data and b) CIVA prediction

What is concluded from the comparison of experimental results and CIVA predictions is that all SDH and most of the notch targets are detected experimentally, their location is affected more by beam bending than the echo predictions CIVA produces, see for instance Figure 51. This tendency is replicated for the other probes.

Amplitude data are presented below.

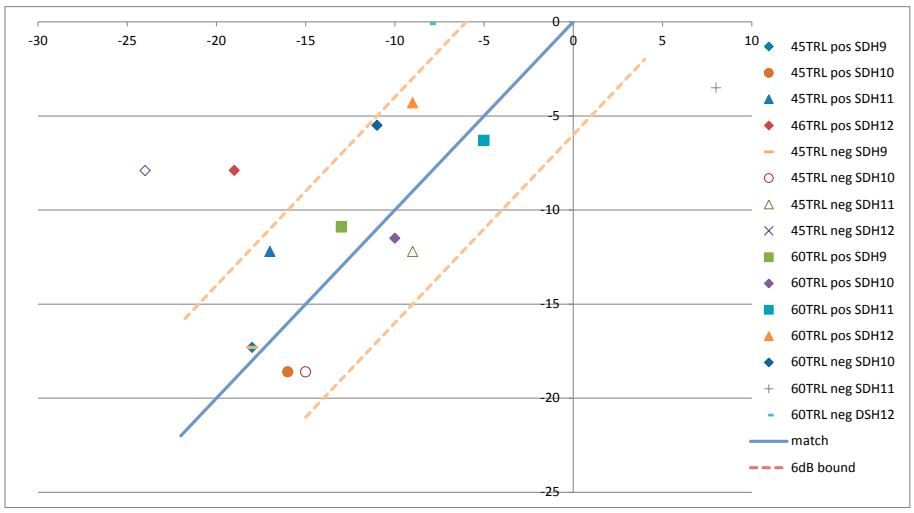

Figure 52 Amplitude data from SDHs with 45 and 60 TRL probes

All measurements are not included in the graph shown in Figure 52. Only measurable signal responses to compare to a CIVA predicted response have been included, as each point in the graph represents the crossing point of the experimental and the simulated results. As shown, most predicted amplitudes match the experiment within ±6dB. Only SDHs are shown in Figure 52. Notch data is presented in Figure 53.

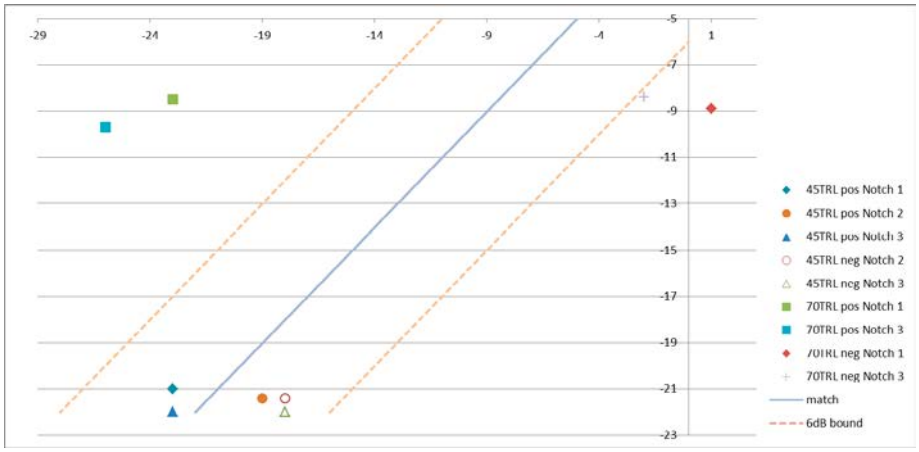

Figure 53 Amplitude data from notches with 45 and 70 TRL probes

The simulations of 45°TRL probes match the experimental data within ±6dB. The 70°TRL predictions are all outside the 6dB bounds. The reason for this has not been addressed.

RAYTRAIM / CIVA Comparison Exercise

AMEC performed a substantial study on inspection performance assessment for a steam generator piping dissimilar metal weld from civil plant (see Figure 54 below). As with the sample shown in Figure 44, the weld joins a ferritic pipe to a stainless steel pipe using nickel-based consumables which results in a strongly textured weld. Relatively speaking, the weld is thick (>80mm thick) and has a large wetted region (region of potentially corrosion crack susceptible material in contact with coolant).

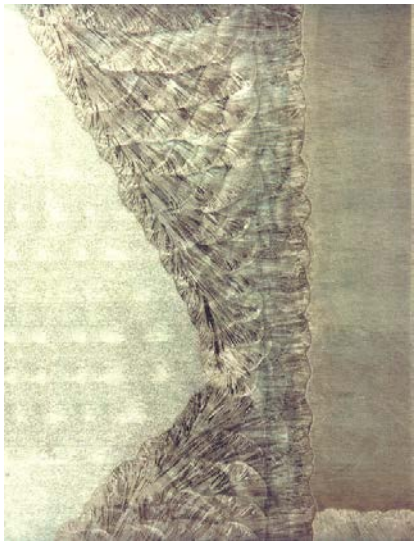

Figure 54 Etched steam generator weld. The section through the component shows the weld (and pipe's) radial/axial section. The surface from which probes could be scanned is the pipe external surface which is located at the top of the figure. Defects of general concern for the inspection are stress corrosion cracking initiating on the internal pipe surface which is located at the bottom of the figure

In-service inspections of these components are generally performed to detect and size any stress corrosion cracking which would initiate on the inner wall wetted region (bottom of weld in figure 54) and grow up through susceptible weld material. The geometry of the weld means that examining beams must pass through relatively large amounts of weld material which is undesirable from the inspection performance perspective as the ultrasonic modelling has to predict the beam bending phenomena that can manifest themselves. It also presented an opportunity to try CIVA on a practical case. Direct relevance to NPP components is limited but this presents a significant if general test of CIVA modelling capability.

RAYTRAIM (ultrasonic ray tracing software) was configured for the examination of longitudinal defects (perpendicular to the viewing plane) with examining beams in the plane of the section; typical CIVA and RAYTRAIM output is shown in Figure 55. The comparison performed was for the beam angles used in the plant item inspection. In summary, results from beam plotting show good agreement on trends. For instance splitting and redirection of beams is closely replicated in modelled cases to the extent that analysis of the results from either model would cause the analyst to come to the same conclusions about regions of poor coverage and maximum beam distortion.

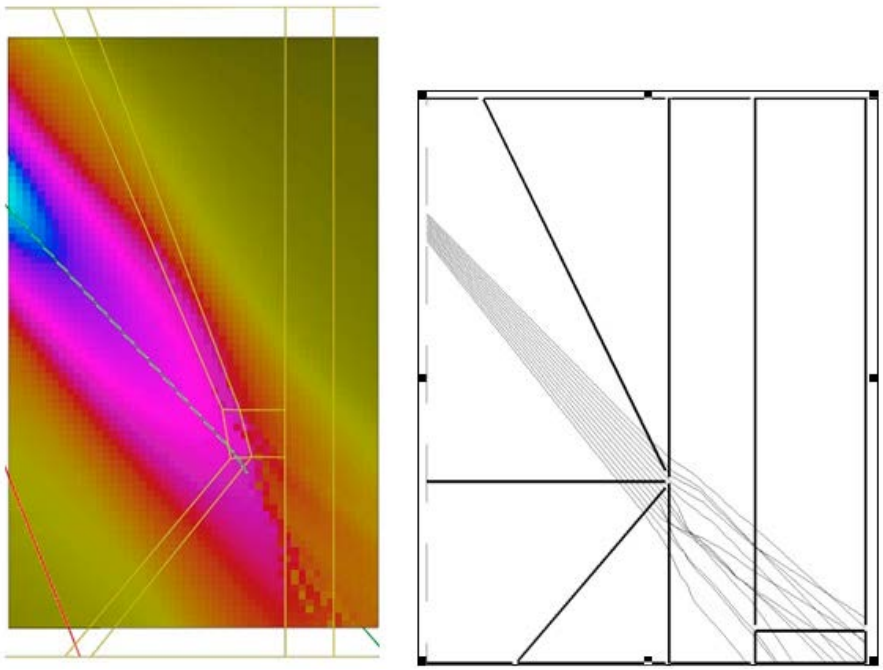

Figure 55 Typical CIVA (a) and RAYTRAIM (b) beam predictions in steam generator weld (Note that CIVA also presents amplitude information)

Note that the configuration of the models to describe the weld region follows different processes. Both models rely on measurement of grain which is encoded in a machine readable form. The CIVA method provides a generally coarser description than the RAYTRAIM. Note also that both models are configured with the same elastic moduli. Thus, there is the possibility of common mode error in this comparison and reliability of results from both models is critically linked to measurements of elastic properties and grain orientation. In both cases, the models require the user

to have a grain orientation map and this must be typical of the weld examined. It is generally possible to generate such grain tables at modest cost. The user needs to be aware that several samples will be required to measure grain orientation with position as this may change (particularly) for site welded plant items. In high integrity plant items, it is not uncommon for there to be welder qualification samples which can be used to obtain grain orientation table data.

Models of grain orientation have been developed and are increasingly used particularly in France. To date these grain orientations have not been assessed in this project.

Conclusions Phase 3

The aim of phase 3 is to assess the performance of CIVA with regards to materials that normally poses difficulties in an inspection situation. Several issues arise here. In a general inspection for example, it is impossible to know the exact structure of the weld. In addition the dendritic growth during solidification of the weld is dictated by both heat flow and gravity, meaning for a site welded pipe for example the structure varies along the weld around the circumference.

The trials that have been made show more pronounced effects on the sound field than CIVA has predicted. A possible reason for this may be that even though the increased beam spread and anisotropy in this type of material has been accounted for, the increased attenuation in weld material has not. As the higher angle part of an angled sound field travels a greater length through material than lower angle sections, this part is affected more by attenuation. This will cause additional beam bending that wasn´t part of the simulations.

Phase 4 experiments

Phase 4 handles rough defect ultrasonic inspection modelling in simple materials.

Currently there are two options of modelling rough defects in CIVA:

1. Using the built-in extension to the plane-defect modelling tool to build a two dimensional section through the defect and then to extrude this in the third dimension.

2. Use of the Athena Finite Element module which is not included in the basic UT modelling package.

Neither option is totally satisfactory for modelling rough defects for different related reasons. Option 1 makes use of the Kirchoff plane defect modelling software and the treatment of roughness out of the plane is partial at best. The software cannot treat the effect of screening of one facet by another nor the contribution made by multiple scattering from the defect surface of diffraction effects. The second method requires an additional investment in software and, while it does include multiple scattering and diffraction effects, makes no allowance for contribution outside of the scattered plane.

Neither AMEC or SQC has purchased the Athena option and what is reported here is an investigation of the use of the inbuilt rough defect modelling tool (option 1 above).

Experimental work

AMEC has conducted a series of experiments to generate data for the comparison experiments reported here. These experiments are based on SCC in stainless steel alloy.

AMEC has developed a method for growing stress corrosion cracks for use in NDE testing and evaluation. The method is known as "MISTIQ" and has been used extensively for generation of test pieces used in operator qualification worldwide.

In this case stress corrosion cracks were grown in stainless steel plate material free from welding.

Morphology Extraction Process Applied to Stress Corrosion Crack Samples

Stress corrosion cracks in general are a more complex defect form which can branch, leave uncleaved regions in the crack plane and can have multiple initiation sites in close proximity. This means in general that it is not possible to 'break' the defect open to reveal a single surface which can be measured in the same way as described above. AMEC have considered a number of possibilities for generation of the surface form. Metallographic sectioning in the plane perpendicular to the defect's length direction reveals the defect's complex form, but only at one length position and experience of multiple sectioning shows that the defect form can vary very rapidly along its length (too rapidly to be practicably obtained by sectioning). Computed tomography has also been investigated as a means for generation of morphology data and whilst this yields useful information about the extent and form of the defect, resolution issues mean some finer detail will be lost. AMEC continues to investigate the best means of obtain necessary morphology data from such defects. However, as remarked above, the defect models currently available within CIVA for treatment of rough defects are only two dimensional. Therefore in this case, the limitation in defect form measurements is of less significance in this exercise than it would be were the models capable of working with a full 3-D representation of the defect form. What has been performed here is extraction of 'facets' by importing pictures of sections through the defect form into a proprietary CAD package (TurboCAD in this instance) and exporting of the facets vertices to build a model in CIVA. The process is complicated and time consuming, but has been performed for a number of defect samples.

A technically preferable geometric technique is to resolve the defect into triangular tiles which has the great benefits that the three vertices of a triangle are always coplanar and it is possible to construct a surface of virtually any complexity with triangles while this is not the case with rectangular tiles.

This approach has been assessed as part of a project by VTT in Finland [5]. The aim was to create realistic simulated data for creation of POD curves. Morphology data was extracted in collaboration with BAM in Germany using their TOMOCAR

equipment for computed X-ray tomography of the defect. TOMOCAR is a system custom built to provide X-ray tomography of welds in piping. The 3-D data from tomography was then imported into MATLAB (MATrix LABoratory, numerical computing software tool) where it was treated in a series of steps to finally be represented as a triangular meshed defect (Figure 56).

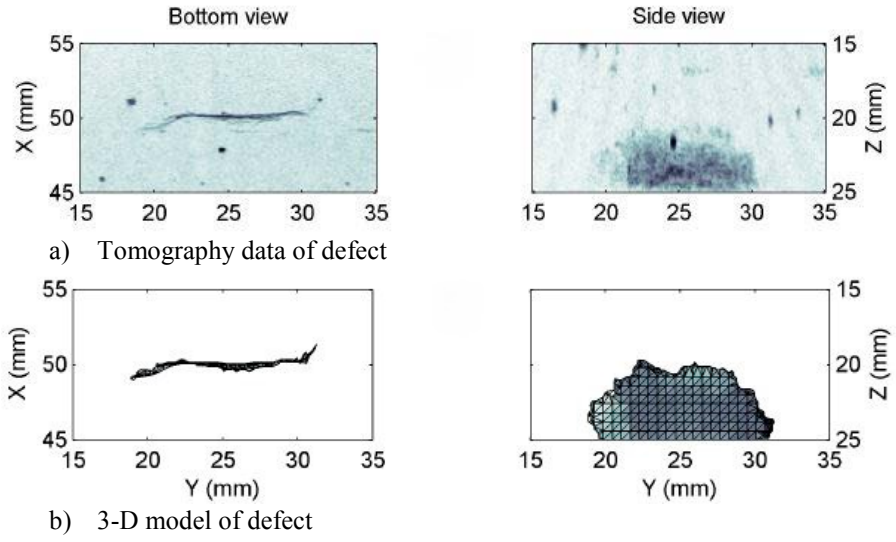

Figure 56 Fatigue defect extracted from a) tomography data to b) triangular tile 3-D defect

The conclusion in the Finnish report is "This indicates that with proper flaw models, CIVA can give realistic results from ISI type of flaws. Moreover, if EDM notch is used in UT simulations, indication amplitude can be almost 6 dB higher than with real ISI flaws."

In the study undertaken for this project, a series of stress corrosion crack samples (as described above) were grown in stainless steel alloy plates. The plates were 32mm thick. Defects with a range of depths were grown and ultrasonic data was collected from them using conventional probes typical of those used in nuclear power plant inspections.

Ultrasonic data were collected with a 2-D raster scan. Once data were collected, the sample was subjected to x-ray computed tomographic inspection at Manchester University and was sectioned. In the study reported here, the crack profile exposed by sectioning was manually digitized by loading a digital photograph of the section in to a CAD- package (TurboCAD in this instance), drawing a polyline on to the profile and extracting the vertices of this polyline. The following figure (Figure 57) shows the extraction process.

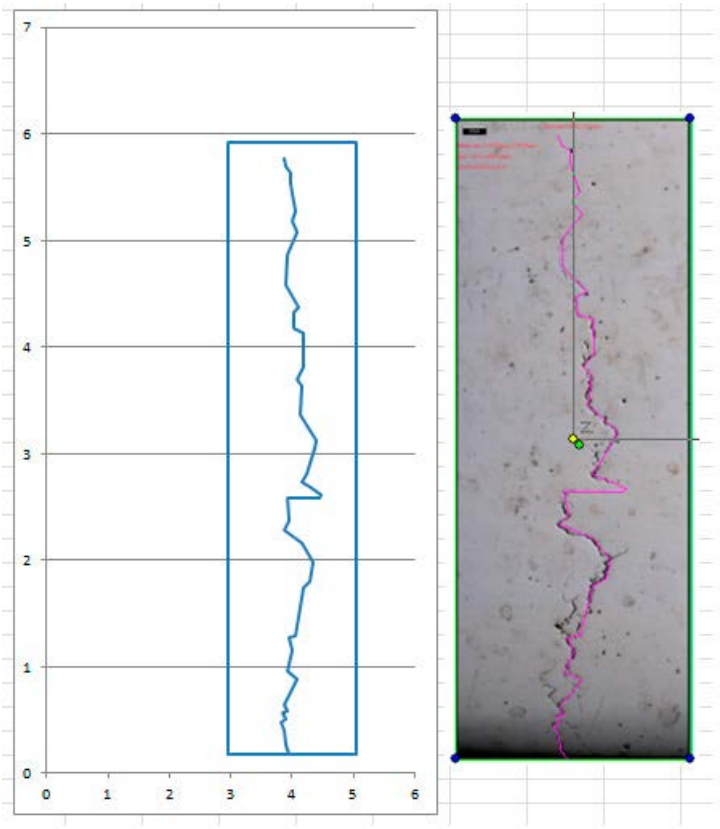

Figure 57 The figure shows the section obtained for sample investigated overdrawn with a polyline (in purple). The left hand figure shows a graph of the graphed vertices

From knowledge of these vertices, a multifaceted defect model has been generated within CIVA. CIVA offers the possibility of simulating defect roughness in the length direction, but this is fairly crude. What has been done in this study is that the defect has been assumed to be uniform in the length direction and the ultrasonic echo data associated with this section has been extracted from the scans which have been performed.

As can be seen from the plot, the manual extraction process loses some of the surface form and some branches have not been included in the polyline. In general the profile is not the same on one side of the defect as it is on the other. Were the crack to have a uniform width, and to be unbranched, the expectation would be the surfaces on each crack surface would be the same. However for this crack species, the width is not uniform and the defect is significantly branched. In the study performed here, separate assessments of the left and right side of the defect were drawn in and the aim when drawing the polyline was to follow the edge or envelope of the defect.

Results and comparison

The specimen which has been modelled contains a vertical smooth slot, a 3mm SDH and the representation of the defect in specimen A which is shown in Figure 57 above. The following image shows the assembly used within CIVA.

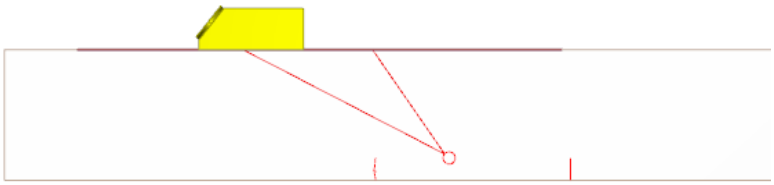

Figure 58 CIVA setup used in evaluation exercise. Order of targets from left to right: SCC, SDH, notch

The arrangement is such that the near field length for the examining probes is about 31mm, hence all targets are strictly outside the near field zone.

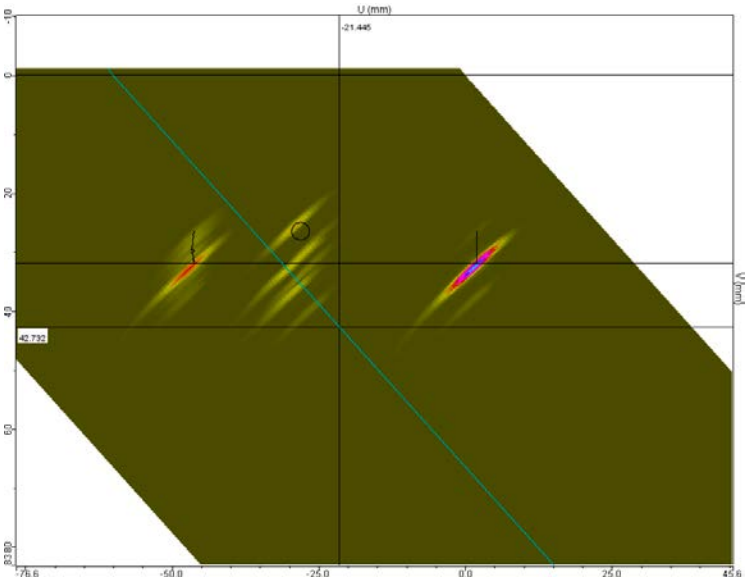

Figure 59 Echo predictions for the 45° shear wave probe case

Note the close packing of the targets within the model has led to some multiple reflections particularly from the SDH to the defects. This does not affect the overall results presented to the conclusions reached, but caution should be exercised when trying to interpret the longer flight time aspects of the temporal prediction.

Echo prediction discussion

In all cases modelled:

- the largest reflector within the modelled set arises from the smooth corner,
- the rough corner yields a smaller but still large echo and
- the rough face yields scattered signal across the entire face which are larger for all probes than the smooth tip response.

These observations are in line with expectation.

Scan	SDH	Smooth corner	Smooth tip	Rough Corner	Rough Face
45° CIVA	-13.4 dB	0 dB	-37.5 dB	-8.1 dB	-21.9 dB
45° expt				0.6 dB to -4 dB	-15 to -20dB
60° CIVA	-14.7 dB	0 dB	-35.1 dB	-6 dB	-20.3 dB
60° expt				-5.1 dB to -8dB	-15 to -20dB
70° CIVA	-10.3 dB	0 dB	-26.9 dB	-7.7 dB	-15.8 dB

Table 10 Tabulated amplitudes

Conclusions Phase 4

There are no crack-like flaws in the flaw library of CIVA. Only artificial flaws such as notches of different shapes, SDH or FBH are available. This may work to some extent if the simulated inspection handles defects with typically a large signal to noise ratio, such as fatigue cracks in base material or carbon steel welds. However these types of flaws are not representative for service induced defects such as stress corrosion cracks.

If done correctly, it is possible to build defects either within CIVA or import defects from external software that will present a credible signal pattern. However, this will require some additional knowledge about the morphology of the defects that are to be expected within the object.

Phase 5 experiments

Phase 5 handles rough defects in difficult materials.

AMEC owned a series of SCC defects in Inconel alloy welds representative of dissimilar metal welds encountered in civil nuclear plant inspection. AMEC also owned ultrasonic data collected from these samples. The aim was to make use of these samples as a basis for establishing the practicability of modelling such a complex scenario in CIVA.

The inspections are dominated by:

- the complexity of the defects,
- the strong attenuation and beam distortion arising from the weld material and transitions in the vicinity of the weld,
- the noise from benign features of the weld – in particular noise from the cladding layer.

The same issues of complexity as discussed in the previous section apply to this defect type. As had been performed in the previous SCC study, defects were cut out of the weld and then subjected to x-ray tomography and then sectioned. As had previously been described, the process is not ideal as it does not enable all the morphology of the defect to be obtained and is extremely labour intensive. That said, for the present level of sophistication of the CIVA model, the method is more than adequate.

The sample modelled was AMEC's DM018 (identity number) transverse SCC defect in a conventional dissimilar metal weld which joins a clad ferritic piece to a stainless steel piece through an Inconel 182 buttering and v-butt weld. The combination of buttering and weld root gives rise to an approximate 20mm width of wetted, potential SCC susceptible Inconel 182 alloy. Transverse defects are limited in length generally to the weld width while the depth can grow all the way through the weld thickness. Thus the depth to length ratios for this defect type with the transverse orientation can be greater than unity.

Defect morphology data was obtained from sectioning principally for this modelling exercise. As an aside, ultrasonic measurement had determined the extent of this defect at about 7mm and the destructive examination showed a depth maximum of about 10mm.The block is 40mm thick (ligament 30mm).

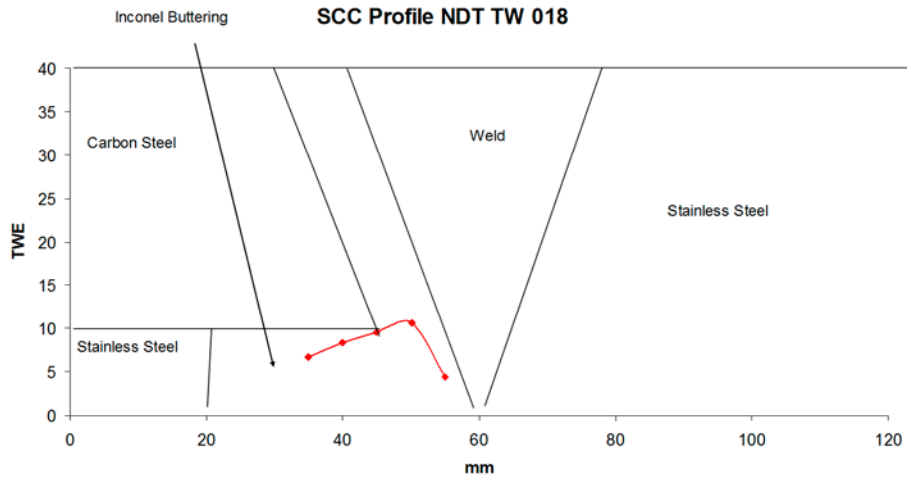

Figure 60 Section information for SCC specimen NDTTW018

For illustration purposes a phased array scan of the defect is shown in Figure 61 below. This shows that while defect is resolvable using advanced inspection technology (central cluster), there is considerable noise in the vicinity of the weld.

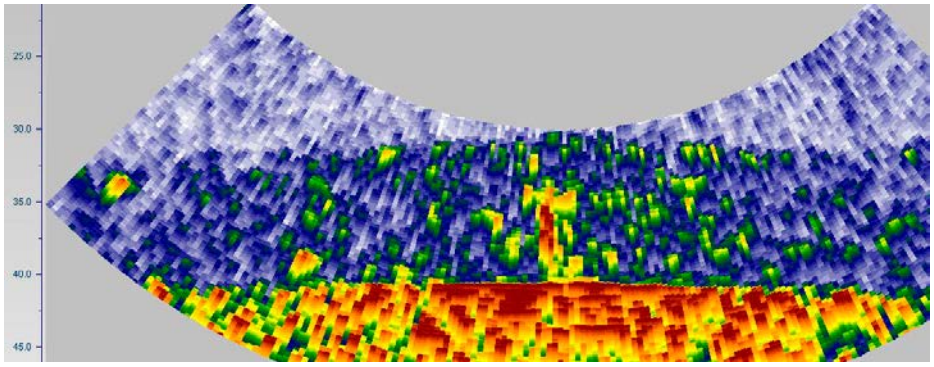

Figure 61 Phased Array B-scan of the defect described above

The simulated set up is described below.

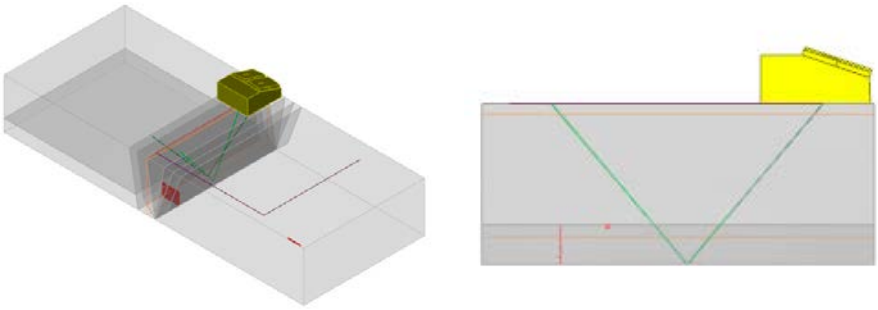

a) b)

Figure 62 a) 3d view of simulated sample and flaw b) side view. Note the calibration reference SDH in the stainless steel parent material. The defect was modelled as an extruded concertinaed series of facets

45 and 60° TRL probes as used in the previous exercise were modelled. In summary, the largest signals were obtained from the rough defect corner with face signals displaced from the corner. In all modelled cases the corner response was predicted to produce a discernible echo within 5dB of the 3mm SDH calibration target response. No echoes associated with the weld transitions or the clad interface was predicted by CIVA.

Conclusions phase 5

Phase 5 is a combination of phases 3 and 4. As discussed in the conclusions of phase 4 the limitations in simulation of beam bending and attenuation provides overly optimistic results. The largest limitation generally however when inspecting these types of object is not beam bending, but rather signal to noise ratio. As noise and attenuation has not been assessed at this stage, the signal to noise ratio predicted by CIVA will naturally be non-conservative estimations.

6. Conclusions

Generally the simulations that has been made matches the experiment rather well. Whether CIVA can be used in qualifications or not is a question of the purpose of the simulation and also the extent of the usage of simulated data.

The differences regarding signal response amplitude between simulations and experiments is in the same order of magnitude as what can be expected between arbitrary ultrasonic operators performing an arbitrary inspection, as seen in the measurement error analysis.

The largest discrepancy between the simulations and experiments in this report, and also in ISI in general is noise, or rather signal to noise ratio. No simulations of noise was made within this project, but is always a significant part of a qualified procedure and the corresponding technical justification. Defects responses are often evaluated in relation to the surrounding noise levels rather than an arbitrary reference target, such as a notch or SDH. Also one need to keep in mind that real defects are individuals, whereas notches are identical. When trying to simulate “real” or “rough” defects within CIVA, a lot of effort has to be put into the work and the result is heavily dependent on the skill of the person creating the defect model.

From a qualification body´s view simulations can be used in two different ways. Either CIVA is used in technical documentation such as a technical justification referring to simulations as a link in the chain of proof to prove that the technique is robust. Or the qualification body may use simulation as a means of controlling or verifying a statement in a technical justification. One can imagine performing parametric studies as a compliment to the measurement error analysis.

The issues discussed above means that it is clear that it is not possible to simulate a complete inspection, or validate an inspection procedure by simulations with CIVA at the current time. The conclusion is that simulations using CIVA can be used when specific problems or technical solutions must be solved or developed.

When used in qualifications, CIVA must be used with great care but together with a well-defined case CIVA can provide a lot of useful information that may be hard to produce experimentally. One has to keep in mind though, that both the producer of simulated data and the evaluator must have great knowledge about the CIVA software to be able to draw the right conclusions from the results. Also, if simulations are to be used in a technical justification, all settings and choices in the simulation setup must be justified just as any setting or choice in the inspection procedure to be qualified, else the qualification body cannot draw any conclusion regarding the statements´ validity.

Future work with validation of cases using the CIVA software can preferably be focused on the topics mentioned above, attenuation and noise. The knowledge gained during this project in combination with the proposed future work would provide a solid ground of experience as a base for more extensive use of CIVA within qualification projects.

References

[1] CIVA 11 User manual, CEA
[2] A. S. Eriksson, A. Boström, H. Wirdelius; Experimental Validation of UTDefect, SKI Report 97:3
[3] WL Daniels, LM Li, SE Wedge, NA Turner, C Aerts; C1-2-2-1 2011 report on CIVA
[4] www.extende.com validation data
[5] J. Haapalainen; RESEARCH REPORT VTT-R-00674-14

2017:29

The Swedish Radiation Safety Authority has a comprehensive responsibility to ensure that society is safe from the effects of radiation. The Authority works to achieve radiation safety in a number of areas: nuclear power, medical care as well as commercial products and services. The Authority also works to achieve protection from natural radiation and to increase the level of radiation safety internationally.

The Swedish Radiation Safety Authority works proactively and preventively to protect people and the environment from the harmful effects of radiation, now and in the future. The Authority issues regulations and supervises compliance, while also supporting research, providing training and information, and issuing advice. Often, activities involving radiation require licences issued by the Authority. The Swedish Radiation Safety Authority maintains emergency preparedness around the clock with the aim of limiting the aftermath of radiation accidents and the unintentional spreading of radioactive substances. The Authority participates in international co-operation in order to promote radiation safety and finances projects aiming to raise the level of radiation safety in certain Eastern European countries.

The Authority reports to the Ministry of the Environment and has around 300 employees with competencies in the fields of engineering, natural and behavioural sciences, law, economics and communications. We have received quality, environmental and working environment certification.

Strålsäkerhetsmyndigheten
Swedish Radiation Safety Authority

SE-171 16 Stockholm
Solna strandväg 96

Tel: +46 8 799 40 00
Fax: +46 8 799 40 10

E-mail: registrator@ssm.se
Web: stralsakerhetsmyndigheten.se

Arkitektkopia AB, Bromma, 2017